
Article:
Mammarappallil, J.G., Rankine, L., Wild, J.M. orcid.org/0000-0002-7246-8660 et al. (1 more author) (2019) New developments in imaging idiopathic pulmonary fibrosis with hyperpolarized xenon magnetic resonance imaging. Journal of Thoracic Imaging, 34 (2). pp. 136-150. ISSN 0883-5993

https://doi.org/10.1097/RTI.0000000000000392

New developments in imaging Idiopathic Pulmonary Fibrosis with hyperpolarized Xenon MRI

Joseph G. Mammarappallil[a], Leith Rankine[a], Ho-Fung Chan[b], Nick Weatherley [b], Jim Wild [b], & Bastiaan Driehuys[a]

[a] Duke University Medical Center, Durham, North Carolina, USA. Department of Radiology. 2301 Erwin Road Box 3808 Medical Center, Durham, NC 27710.

[b] University of Sheffield, Western Bank, S10 2TN, United Kingdom

Abstract

Idiopathic Pulmonary Fibrosis (IPF) is a progressive pulmonary disease that is ultimately fatal. While the diagnosis of IPF has been revolutionized by high resolution computed tomography (HRCT), this imaging modality still exhibits significant limitations, particularly in assessing disease progression and therapy response. The need for non-invasive regional assessment has become more acute in light of recently introduced novel therapies and numerous others in the pipeline. Thus, it will likely be valuable to complement 3D imaging of lung structure with 3D regional assessment of function. This challenge is well addressed by hyperpolarized (HP) ^{129}Xe magnetic resonance imaging (MRI), exploiting the unique properties of this inert gas to image its distribution, not only the airspaces, but also in the interstitial barrier tissues and red blood cells (RBCs). This single-breath imaging exam could ultimately become the ideal, non-invasive tool to assess pulmonary gas-exchange impairment in IPF. This review article will detail the evolution of HP ^{129}Xe MRI from its early development to its current state as a clinical research platform. It will detail the key imaging biomarkers that can be generated from the ^{129}Xe MRI exam, as well as their potential in IPF for diagnosis, prognosis, and assessment of therapeutic response. We conclude by discussing the types of studies that must be performed for HP ^{129}Xe MRI to be incorporated into the IPF clinical algorithm and begin to positively impact IPF disease diagnosis and management.

Commented [RLJ1]: R.1.1

Introduction

Idiopathic pulmonary fibrosis (IPF) is the most commonly encountered form of pulmonary fibrosis[1]. The disease typically presents with progressive dyspnea and has historically had a grave prognosis, with a median survival of only 3-5 years[2,3]. However, where the disease was once thought of as a true "death-sentence", the recently approved therapies, nintedanib and pirfenidone, have provided new hope for patients[4–9]. These new chemotherapeutics have demonstrated the ability to slow the decline of pulmonary function while improving progression-free survival[6,7,9]. However, the introduction of these medications have placed a premium on the need for accurate and timely diagnosis of IPF from other fibrotic or chronic pulmonary diseases[10], as well as better staging. Moreover, the high cost of these medications of up to $100,000 per year and related side effects also introduces the need to quickly determine which patients are benefitting and which are not[11].

An initial evaluation of patients with shortness of breath typically begins with a visit to a pulmonologist who obtains a relevant history, performs a physical examination, and obtains pulmonary function tests (PFTs). Patients with IPF often demonstrate restrictive physiology[12,13], quantified by diminished forced vital capacity (FVC), and a reduction in diffusing capacity of carbon monoxide (DL_{CO}). However, this evaluation, in isolation, cannot be used to diagnose IPF, as it must be distinguished from a group of over 200 interstitial lung diseases (ILDs), many of which present clinically in a similar fashion. Moreover, global pulmonary function testing is relatively insensitive to early disease and can be confounded by comorbidities. For example, patients with early fibrotic lung disease or combined pulmonary fibrosis and emphysema (CPFE)[14–16] often do not demonstrate restriction on PFTs. As the disease is "idiopathic" by definition, the diagnosis necessitates investigation for any potential etiology of pulmonary fibrosis excluding the diagnosis of IPF[3].

Beyond pulmonary function testing, diagnostic imaging, in the form of high-resolution computed tomography (HRCT), has revolutionized evaluation of fibrotic lung disease. HRCT imaging findings are currently a mainstay in IPF diagnosis[17], with The American Thoracic Society recommending that fibrotic lung disease be categorized into 3 diagnostic groups: usual interstitial pneumonia (UIP) pattern, possible UIP pattern, and inconsistent with UIP. The UIP pattern of disease is identified on HRCT by a basilar predominance of subpleural reticulations and honeycombing, an absence of features considered inconsistent with UIP pattern, and, commonly, traction bronchiectasis[17]. Although all of these imaging findings may be seen in a majority of cases, it is the presence of honeycombing that is essential to assign a UIP pattern of fibrosis. This pattern, in the absence of an etiology for fibrosis, is sufficient to assign a diagnosis of IPF and begin treatment with novel drugs. However, 30-40% of patients eventually diagnosed with IPF do not exhibit a UIP-pattern on CT at presentation[18]. Instead, their imaging findings often reveal a possible UIP pattern (basilar predominant findings without honeycombing), which can represent early IPF, other fibrotic lung disease, or senescent change[19,20]. Such cases of possible UIP, without definitive imaging findings, and frequently confusing patient histories, are often presented at multidisciplinary conferences to generate consensus regarding an IPF diagnosis. In many cases, patients will undergo surgical lung biopsy to obtain histopathologic assessment of disease, yet this group of patients is at high risk for post-biopsy ventilator dependence and air leak[18]. Furthermore, the additional time required to reach specialist consensus and/or acquire a lung biopsy directly delays the initiation of therapy.

Commented [RLJ2]: R.1.2

Commented [RLJ3]: R.1.3

Although IPF ultimately progresses to respiratory failure, its natural progression is often insidious, with a disease course that is highly variable across patients[21] (Figure 1). While many patients die within 2-3 years of diagnosis, approximately 20-25% live more than 10 years[22]. This wide variability emphasizes

the need to identify patients in a timely, efficient manner to potentially halt disease progression by appropriate therapy from the evolving drug repertoire.

In addition to the diagnostic challenges of IPF, monitoring disease progression has proven to be difficult with currently available techniques. Although, PFTs including forced vital capacity and diffusing capacity of the lung (DLco) are typically used clinically to assess the respiratory and gas exchange limitations that accompany IPF[5], these methods have significant limitations. For example, it has proven difficult to standardize DLco in multicenter trials and there remains a lack of agreement for values of FVC to identify significant pulmonary decline and initiate treatment[23,24]. Moreover, while CT plays a critical role in the diagnosis of IPF, it has fared less well in detecting disease progression or therapeutic response. Multiple studies have attempted to use single-time-point, as well as serial CT scans to assess therapeutic response and disease progression[25–28]. Unfortunately, these studies have not yet come to a consensus on whether structural findings of fibrosis are correlated with clinical disease progression[29]. Nonetheless, emerging quantitative CT methods, including density-histogram and texture analysis, as well as machine learning, have shown promise in more strongly connecting structural features to clinical disease progression[30–33].

Commented [RLJ4]: R.2.5

Commented [RLJ5]: R.1.4

Commented [RLJ6]: R.2.6

It is clear that the currently available clinical tools present IPF clinicians with a combination of challenges when it comes to definitive diagnosis, prognosis (i.e. selection for anti-fibrotic drugs), and early detection of patient decline or therapy response. These unsolved clinical challenges motivate the hunt for other non-invasive measures of pulmonary function in IPF. One such promising non-invasive measure is hyperpolarized xenon-129 (HP ^{129}Xe) magnetic resonance imaging (MRI), which, as will be described in this review, permits quantitative mapping of 3-dimensional (3D) lung function. This functional lung imaging technique provides a unique series of potential solutions to some of the most

Commented [RLJ7]: R.2.2

challenging diagnostic and prognostic problems in IPF. The purpose of this review will be to discuss the evolution of HP ^{129}Xe MRI as a means to evaluate IPF, from its early development to its current, limited clinical dissemination. This article will provide background on the challenges of imaging the lungs by MRI, describe the unique properties of ^{129}Xe that address these challenges, and describe the key imaging biomarkers that can be generated from ^{129}Xe-MRI, and their potential for use in diagnosis and longitudinal assessment of disease progression. Ultimately, we will argue that the ability to non-invasively, rapidly image the distribution of an inhaled, inert gas and to quantify its 3-dimensional distribution into the lung airspaces, interstitial barrier tissues and capillary blood, provides promising, new, spatially resolved biomarkers that could address many of the long-standing diagnostic and prognostic challenges in IPF. However, given the emerging nature and rapid evolution of this technology, we close by outlining the types of studies that must be designed and executed so that this unique technology can begin to impact on the way patients with IPF are cared for.

Commented [RLJ8]: R.2.7

Commented [BD9]: R.2.1

Magnetic Resonance Imaging of the Lungs

Commented [RLJ10]: R.2.8

Magnetic Resonance Imaging (MRI) has not traditionally been thought of as a modality to evaluate pulmonary structure-function. The lungs' low proton density and poor magnetic susceptibility environment caused by ubiquitous air-tissue interfaces generally defy conventional gradient and spin-echo proton (^{1}H) imaging approaches. The low and slowly recovering signal, coupled with short T2* relaxation times cause MR images of the pulmonary parenchyma to appear as void spaces. To a certain extent this can be overcome with emerging respiratory-gated ~4 min long free-breathing Ultrashort Echo Time (UTE) acquisitions that considerably improve structural delineation[34]. However, while representing a significant advance (Figure 2), these sequences do not yet achieve the 1mm voxel inspiratory structural resolution required to delineate reticulation[17]. Moreover, structural findings alone will likely be limited in characterizing disease severity and progression[13,35].

Commented [RLJ11]: R.1.5

Over the past several decades, the introduction of gaseous, non-proton, inhaled contrast agents has opened a new window of opportunity for MR imaging of pulmonary function[36,37]. Importantly these agents have no endogenous background signal, which facilitates the ability to directly visualize their distribution within the lung. Historically, gases have been considered virtually impossible to image directly by MRI, owing to a density that is 10,000 times lower than that of tissues. One exception to this is perfluorinated agents, which employ a high density of ^{19}F nuclei, large magnetic moment, and short T_1 recovery to enable their distribution to be imaged at thermal equilibrium. However, the majority of work to date has employed the so-called hyperpolarized gases[36] – ^{3}He and ^{129}Xe. These are both inert, noble gases with nuclear spin 1/2, and can have their nuclear spin alignment increased by ~100,000-fold compared to thermal equilibrium attained in the magnetic fields typical of MRI. This process is known as "hyperpolarization" and overcomes the low density of these gases to enable imaging them rapidly, at high-resolution, and in a single breath-hold. This technology was originally advanced using hyperpolarized (HP) helium-3 (^{3}He), which demonstrated high-resolution imaging of pulmonary ventilation[38,39] as well as tissue microstructure via the apparent diffusion coefficient (ADC)[40,41]. The technology has been extensively applied to gain new insights into diseases where the underlying pathology resides primarily within the airways and airspaces[42,43].

However, over the past decade, MR imaging with hyperpolarized gases has transitioned away from ^{3}He due to its limited availability (it is produced as a by-product of tritium decay), as well as its rapidly rising cost. This has turned attention to ^{129}Xe as the more sustainable hyperpolarized signal agent. ^{129}Xe is a stable isotope of xenon, making up 26% of its natural abundance and is derived from the earth's atmosphere as a natural part of the air separation process. Its development initially lagged that of ^{3}He owing to a magnetic moment that is roughly 3-fold lower and slightly less mature hyperpolarization technology. However, this has recently been overcome with a series of technology advances and ^{129}Xe

has been shown capable of high-resolution ventilation imaging[38]. Moreover, its unique properties are now recognized as holding the key to imaging pulmonary gas exchange in IPF.

Hyperpolarization: making ^{129}Xe visible on MRI

^{129}Xe is typically hyperpolarized using the spin exchange optical pumping technique, yielding gas polarization levels of 20-50%. Moreover, modern hyperpolarization methods are able to generate these polarization volumes rapidly, at rates of (1 -3 L/h)[44] . The hyperpolarized state of ^{129}Xe, when contained within specialized perfluoropolymer delivery bags, persists for a relatively long time with T1 relaxation of ~1-2 hr, permitting the gas to be stored for several minutes and delivered to the patient without undue hurry. However, once it is inhaled and comes in contact with oxygen, which is paramagnetic and thus depolarizing to ^{129}Xe, the gas must be imaged quickly as its T_1 relaxation time decreases to ~20-30 sec. However, this does not impose a substantial limitation, since scans are conducted within a single breath-hold of typically less than 15 sec. Moreover, patients can undergo imaging even if they require supplemental oxygen to be delivered via nasal cannula. That is because they inhale orally from the dose delivery bag, and thus ^{129}Xe does not mix with O_2 until it enters the lungs. Prior to delivery, HP ^{129}Xe is commonly mixed with ultra-pure nitrogen gas to provide a standardized 1 L inhalation. Note that this approach is technically simpler and more readily achievable in practice, although certain quantitative imaging methods recommend adjusting the volumes to 15% of total lung capacity[45]. Although xenon is an anesthetic when breathed continuously in sustained concentrations, the smaller doses used for MRI have been demonstrated in adults and children to have minimal, transient analgesic effects that are well-tolerated and clear rapidly after the breath-hold[46–48].

Commented [RLJ12]: R.2.9

Commented [RLJ13]: R.2.10

The magnetic resonance properties of ^{129}Xe are relatively favorable for MRI. It is a spin ½ nucleus with a gyromagnetic ratio of ^{129}Xe is -11.78 MHz/T, a factor of 3.61529 smaller than for ^{1}H, leading to resonant frequencies of ~17.7 and 35.3 MHz at 1.5 and 3.0 T, respectively. Within the gas phase in the lung's airspaces, it benefits from its lower resonant frequency and diffusional motional narrowing, both of which ameliorate the rapid dephasing experienced by static protons in lung tissues. Thus, despite the magnetically inhomogeneous environment of the lung, gas-phase ^{129}Xe T2* values are typically 10's of milliseconds, even at 3 Tesla[49] and permit ventilation imaging using simple, fast gradient echo sequences. Moreover, given that the hyperpolarization of ^{129}Xe occurs outside of the magnetic field, the technology performs equally well at 1.5T and 3T[49]. Nonetheless, the requirement for rapid breath-hold imaging, has led to continued substantial MR physics research to develop both novel RF coils[50,51] and image acquisition pulse sequences[52,53] that provide maximum imaging detail in minimal time.

Like all non-proton imaging, ^{129}Xe MRI requires scanners equipped with multi-nuclear capabilities. This includes additional RF hardware and software that is typically offered as an add-on feature by the major MRI manufacturers, adding ~15% of the base cost of the scanner. In addition, institutions must purchase and maintain a xenon polarization system and associated QA diagnostics, at a cost of ~$500k. Operation of these systems may require up to 1 full-time-equivalent technologist, depending on clinical load. Beyond these upfront costs, the primary consumables used in HP gas MRI are the ^{129}Xe gas and the dose bags used to administer the agent to patients.

Commented [RLJ14]: R.2.11

^{129}Xe Ventilation and Diffusion-Weighted Imaging

Commented [RLJ15]: R.2.12

The simplest and most well-established hyperpolarized ^{129}Xe image is one that maps its ventilation-driven distribution within the lungs. Early work comparing such static ventilation images between ^{129}Xe and ^{3}He MRI revealed that the higher density of ^{129}Xe appears to make it even more sensitive to ventilation defects[38,54]. Although ventilation abnormalities are not considered to be the predominant

feature of IPF, ^{129}Xe ventilation MRI does reveal subtle patterns of ventilation heterogeneity and airway dilation related to traction bronchiectasis (Figure 3). Moreover, a careful quantitative analysis of ventilation patterns appears to show some sensitivity to disease stage as measured by the gender, age and physiology (GAP) index[55].

Like ^{3}He, the free-diffusion of ^{129}Xe within the lungs airspaces is restricted by its natural microstructure. This opens up the second, well-established contrast mechanism: diffusion-weighted imaging. That is, by acquiring gradient-refocused images after applying diffusion-sensitizing gradients, the restricted motion is encoded to reveal possible airspace enlargement. While this has primarily been applied to the measurement of regional emphysema in patients with COPD[56], this contrast mechanism is also sensitive the enlarged acinar dimensions and cystic spaces that arise in the fibrotic lung. This is illustrated in Figure 4, showing significantly elevated ^{129}Xe apparent diffusion coefficient in regions of traction bronchiectasis and honeycombing in patients with IPF[53]. These airspaces are larger than are found in the normal lung, thereby allow ^{129}Xe to diffuse over larger distances within them. Note that, in this context, diffusion refers to classic Brownian motion within the airspaces, not the classical physiological notion of gas diffusion across the blood gas membrane, denoted as “gas exchange”, to be addressed in the remainder of the manuscript.

Unique Properties of ^{129}Xe to Enable Gas Exchange Imaging

While it is perhaps remarkable that ventilation and ADC imaging exhibit sensitivity to some aspects of pulmonary fibrosis, IPF is primarily defined by heterogenous, fibrotic thickening of the interstitial barrier tissue and alveolar collapse[57] that collectively impair gas exchange. These aspects of pulmonary physiology can be more directly probed by exploiting the diffusivity, blood solubility, and frequency shifts of ^{129}Xe[58]. Collectively, these properties are what drive the unique capability of ^{129}Xe to essentially image the gas exchange pathway followed by inhaled oxygen[59].

Commented [RLJ16]: R.2.13

Upon inhalation into the alveolar space, xenon diffuses across the alveolar-capillary barrier membrane, where it exhibits a distinct shift in its resonant frequency by roughly 197.8 parts per million (ppm)[60] relative to ^{129}Xe atoms remaining in the airspaces. This translates to a readily detectable shift of ~3.5kHz at 1.5 Tesla. From here, it passes into the local capillary network and enters into the red blood cells (RBCs) where it exhibits an even larger frequency shift of 217.6 ppm[60]. These two compartments, barrier and RBC, are collectively referred to as the "dissolved-phase", with the spectral structure depicted in Figure 5. This figure also illustrates the inherent challenge of imaging ^{129}Xe in the dissolved phase, with a signal that is only 1-2% as large as that of the gas phase. However, in 2010, Cleveland et al, recognized that this small signal was continuously replenished by ^{129}Xe diffusing in from the airspaces and thus could be encoded using substantially larger flip angles than used for conventional ventilation imaging. This approach allowed nearly the entirety of the inhaled ^{129}Xe magnetization to be used to image dissolved-phase ^{129}Xe 3-dimensionally in human subjects[61] (Figure 6). In that same year, Mugler and co-workers demonstrated that dissolved and gas-phase ^{129}Xe could be imaged in the same breath-hold[62], a capability that would ultimately prove critical for enabling quantitative analysis of gas transfer.

Imaging the dissolved phase signal from ^{129}Xe the lungs is technically challenging, owing not just to its relatively weak signal, but also to the very short transverse relaxation time,$T2^*$, of ^{129}Xe in the interstitial barrier and RBCs (~2 ms at 1.5 Tesla[63]). This is because the poor susceptibility environment of the lung is no longer mitigated by rapid motion available to gas-phase ^{129}Xe. As such, the short-lived transverse ^{129}Xe magnetization must be rapidly encoded using imaging sequences with short echo times such as 3D radial acquisitions. Such radial sampling [64–66] is also inherently robust against motion and, because the radial views can be acquired in randomized order, images can be reconstructed even if the patient is unable to complete the full breath-hold. Thus, so long as patients meet the requirements to undergo MRI, the ^{129}Xe MRI exam should be well-tolerated and relatively independent of breath-hold capability.

HP ^{129}Xe Spectroscopic Signatures in IPF

The first indications that hyperpolarized ^{129}Xe could be a sensitive probe in IPF used a simple whole-lung spectroscopic indicator of xenon uptake in barrier and versus RBCs. In 2014, Kaushik et al[67] found that the signal arising from ^{129}Xe in RBCs was significantly reduced in patients with IPF compared to healthy volunteers (Figure 7). This was quantified in the ratio of RBC to barrier signal and was found to be significantly lower in a group of six IPF subjects (0.16 ± 0.03) compared to 11 healthy volunteers (0.55 ± 0.13, P<0.0002). In this small cohort, the RBC to barrier ratio was found to correlate exceptionally well with DL_{CO} (r = 0.89, P < 0.0001). Subsequent work has provided standardized spectroscopic curve fitting tools and suggested the barrier resonance to potentially consist of more than a single resonance, but verified the strong DLco correlation[68]. In fact, the ability to measure diffusion limitation with xenon, a gas traditionally taught in physiology to be "perfusion-limited", is explained by the unique properties of hyperpolarized ^{129}Xe detection and its inherent localization to the alveolar capillary interface[69]. Notably, although, like DL_{CO}, the RBC:barrier ratio is a global metric, it does not require a precisely timed breathing maneuver and can be measured continuously every 20 ms, which therefore may confer it with higher reproducibility. Importantly, the average RBC:barrier ratio will depend somewhat on the combination of TR and flip angle used for the acquisition and thus these parameters should be standardized in order to facilitate comparison across sites.

As an alternative to obtaining a single, steady-state ^{129}Xe spectrum, it is also possible fully characterize the dynamics of ^{129}Xe gas transfer across the blood gas barrier. This method is known as the ^{129}Xe chemical shift saturation recovery (CSSR) technique[70], a time resolved spectroscopy sequence. Using this approach, Stuart et al compared xenon uptake kinetics and models of lung microstructure in 10 healthy volunteers with 4 IPF patients and 4 patients with systemic sclerosis (SSc)[71]. This work was able to estimate septal thicknesses of 10.0 ± 1.6 µm for healthy volunteers, 13.0 ± 1.5 µm for subjects with SSc

and 17.2 ± 1.1 µm for patients with IPF. In a preliminary study assessing the repeatability of extracting such microstructural parameters found it to be roughly equivalent to that of the DLCO lung function test[72].

Development of HP ^{129}Xe Gas Exchange MRI to Spatially Resolve Barrier and RBC

While demonstrating the sensitivity of ^{129}Xe spectroscopy to impaired gas exchange in IPF was an important milestone, it was also recognized that improved sensitivity to disease progression and therapy response would require resolving this differential uptake spatially. In fact, spatially resolved imaging of impaired gas transfer had been demonstrated roughly a decade earlier in a rat model of fibrosis[73]. This work used a simple 1-point Dixon-based method that separates the ^{129}Xe barrier and RBC images by encoding the center of k-space when the two compartments are 90° out of phase. Although limited to only 2D planar acquisition, this early work demonstrated that ^{129}Xe transfer to RBCs was severely diminished in the left lung, which had been unilaterally instilled with bleomycin. This was eventually extended to 3D imaging in work that also provided a strong theoretical underpinning for the ability of hyperpolarized ^{129}Xe MRI to image imparied gas exchange[69]. Once the dissolved phase imaging of xenon had been demonstrated in human subjects, the stage was set for the pioneering work of Qing et al to demonstrate 3D, fully separable imaging of ^{129}Xe in airspaces, its uptake in barrier tissues and transfer to RBCs in a single breath[64] (Figure 8). This work, conducted at 1.5 T, used 4 echoes acquired via a 3D radial trajectory to enable hierarchical IDEAL-based [74] decomposition of ^{129}Xe in the airspace, barrier and RBC compartments.

Commented [RLJ17]: R.2.14

The initial efforts of Qing et al, applied 3D imaging of ^{129}Xe gas exchange to healthy volunteers, smokers, and asthmatics. Subsequently, Kaushik and colleagues demonstrated an approach using interleaved 3D radial sampling of gas- and dissolved phase ^{129}Xe, along with the more-straight-forward 1-point Dixon-based decomposition to image these three compartments[65]. This method used only a single, short-echo

time acquisition to accommodate the rather short T2* of ^{129}Xe in interstitial barrier and RBCs, which is ~2 ms at 1.5 Tesla[63]. Notably, in addition to healthy volunteers this study also included patients with IPF and revealed features similar to what had been see in in early preclinical bleomycin rat models[73]. The primary signatures were areas of regionally impaired transfer to RBCs[65], which were spatially correlated with areas of fibrosis on HRCT, and appeared to follow a peripheral and basilar pattern (Figure 9).

Quantitative 3D Mapping of Lung Function: Ventilation, Barrier Uptake, and RBC Transfer

The ability to image the ^{129}Xe distribution 3-dimensionally in the lung airspaces, interstitial alveolar barrier, and capillary RBCs, makes it uniquely suited to characterize all of the key functional and structural aspects of lung pathophysiology in IPF. Although the functional images themselves are resolved at the level of several millimeters, they inherently probe the alveolar capillary interface, thereby conferring them with sensitivity to micron-scale thickening of the interstitial barrier[73,75]. These properties are clearly advantageous for assessing IPF where interstitial thickening is a characteristic feature. However, the images obtained by MRI are inherently qualitative (i.e. unitless) and thus require additional transformation to render them into quantitative 3D maps of ventilation, barrier uptake, and RBC transfer. Such maps should then enable comparison across patients and timepoints.

As first proposed by Qing et al, one approach to generating quantitative maps is to divide the barrier uptake and RBC transfer, on a voxel-by-voxel basis, by the "source" signal in the airspace compartment[64]. In this way, differences in ^{129}Xe polarization and inhaled volume are normalized out. Building upon this notion, Z. Wang et al proposed depicting these quantitative ratios as color maps based on intensity histograms derived from a healthy reference population[60] (Figure 10). This was an extension of earlier work by He et al who first used such an approach to quantify the regional ventilation distribution into color bins. In this framework each color bin is given a width that that is one standard deviation of the distribution derived from a cohort of 12 healthy volunteers[76]. This approach defines

"signal defects" as those with an intensity falling more than 2 standard deviations below the mean of the reference population. Applying this algorithm to ^{129}Xe gas transfer MRI allows both defects as well as regions of signal enhancement to be visualized in all three compartments. Such maps can then be used for quantitative analysis by using the relevant percentage of the lung that each bin comprises.

Gas Transfer in Normal Populations vs. Pulmonary Fibrosis

The implementation of the color mapping approach made it possible to observe that functional patterns in IPF patients involved, not only focal defects in RBC transfer, but also that uptake of ^{129}Xe in the interstitial barrier tissues was strongly enhanced[60] (Figure 11). Although, in many patients, enhanced barrier uptake was seen throughout the lung, it was most dramatically increased in the peripheral and basilar regions of the lung. By contrast, such barrier uptake was diminished in many patients with COPD, reflecting the emphysematous destruction of lung tissue leading to a loss of gas exchange surface area. Thus, the addition of quantitative mapping of ^{129}Xe barrier uptake permits visualization of two important aspects of lung microstructural integrity – septal thickness and gas exchange surface area.

> *Subsequently, J. Wang et al applied this quantitative ^{129}Xe gas exchange MRI approach to a larger cohort of patients with IPF as well as correlating these images to pulmonary function testing and HRCT[77]. Interestingly, all ^{129}Xe metrics of ventilation, barrier uptake, RBC transfer, and RBC/barrier ratio, correlated poorly ($r<0.3$) and insignificantly ($P>0.4$) with CT fibrosis scores. But in stark contrast, the ^{129}Xe gas exchange imaging metrics, when averaged over the whole lungs, correlated significantly ($P < 0.05$) with both FVC and DLco. Indeed, as had been observed in prior spectroscopic studies[67], the strongest correlation was between global RBC:Barrier and DLco ($r = 0.94$, $P < 0.01$) as seen in Figure 12. This again confirms the connection of the ^{129}Xe-derived metrics of gas exchange to those rooted in more established physiology. This combination of strong correlations with physiology, coupled with poor correlations to CT is perhaps the clearest indicator that imaging the functioning of the alveolar-capillary unit could provide an important additional disease assessment in IPF. As seen in Wiley*

Figure 13, the ability to identify regionally distinct functional patterns by ^{129}Xe MRI may be indicative of its ability to identify disease that is not yet readily evident on HRCT. In fact, this is perhaps supported by the seminal work of Coxson et al, who showed that even areas appearing normal on CT exhibit extensive

disease at the histological level[75]. It suggests perhaps that the structural abnormalities seen on HRCT, while valuable for establishing a diagnosis of IPF, may in fact be relatively insensitive to the underlying pathologic progression of fibrotic disease.

Detecting Disease Progression and Therapy Response

Commented [RLJ18]: R.2.3

> *Given its ability to visualize functional patterns in IPF, a natural question is whether ^{129}Xe gas exchange MRI may ultimately prove able to detect disease progression and/or therapy response at earlier timepoints than conventional metrics. Recent work along these lines show promise, as Chan et al employed whole-lung ^{129}Xe spectroscopy to detect rapid disease progression in IPF. This study established that the baseline RBC:barrier ratio measured in 10 IPF patients was highly reproducible (ICC 0.96) and that this metric declined significantly over a 6-12 month. Importantly, such decline was not evident in either FVC or DL_{CO}, providing preliminary evidence that ^{129}Xe gas exchange spectroscopy may detect such changes sooner than conventional metrics[78] (Wiley*

Figure 14). Clearly, demonstrating such sensitivity will require comparing these metrics of disease progression with independent measures of clinical outcomes.

The high reproducibility of whole-lung spectroscopy and observed temporal changes in RBC:barrier ratio provides encouragement that, when the barrier and RBC components are resolved spatially, we may also see regional changes in lung that elude traditional PFTs. Although such longitudinal imaging studies only now getting underway, a tantalizing case is presented in Figure 15 depicting a patient who started on anti-fibrotic treatment 1 month before baseline MRI and returned 5 months later for a follow-up scan. At baseline, the patient presented with 49% of their lung volume exhibiting high barrier uptake, while focal RBC transfer defects at the lung bases accounted for low RBC transfer in 35% of the lung. Upon return 5 months later, the percentage of lung exhibiting high barrier uptake had improved to encompass only 30% of the lung, while the RBC transfer defects remained stable at 35% of lung volume. While this single case is clearly anecdotal, it provides a potential view of what therapeutic response imaging could look like in larger cohorts and provides encouragement that, in future, the effects of anti-fibrotic drugs could potentially be spatially assessed, at least in a subset of IPF patients. Clearly larger

scale studies are needed to ultimately link the significance of these spatially resolved changes in functional images to actual clinical outcomes.

Future Directions for HP ^{129}Xe in Evaluating Fibrotic Lung Disease

Given that the distribution of ^{129}Xe from airspaces to interstitial barrier to the capillary RBCs, traces the same gas exchange pathway as that followed by oxygen, HP ^{129}Xe MRI represents a potentially powerful technique to evaluate the regional functional consequences of fibrotic lung disease. The thickening of barrier tissues in early disease likely occurs on a spatial scale of only microns and is thus undetectable using anatomical imaging, even by the exquisite spatial resolution of HRCT. Thus, paradoxically, while the true spatial resolution of ^{129}Xe MRI is modest in comparison, its *functional* resolution by virtue of its sensitivity to diffusion across the blood-gas barrier makes it uniquely sensitive to disease. Ultimately, with further clinical development, this novel MRI technique could be advantageous on many levels of IPF care including diagnosis, prognosis, and therapeutic response.

The diagnosis of IPF remains challenging, but work now underway will help determine whether ^{129}Xe MRI could ultimately play a role in this arena. If a diagnostic pattern could be identified and evidence could be gathered for a high level of diagnostic accuracy, ^{129}Xe MRI could make a significant impact by avoiding the need for risky and more costly surgical lung biopsies. In fact, its true utility for diagnosis would likely need to be demonstrated in patients with earlier stage disease, and those not exhibiting the classic diagnostic UIP pattern on CT. To achieve this goal would require identifying a ^{129}Xe imaging profile that is distinct from other commonly encountered ILDs, such as non-specific interstitial pneumonias (NSIP). To date, studies have demonstrated that IPF patients exhibit high barrier uptake, accompanied by diminished transfer to the RBCs. Notably, both these findings follow a peripheral and basilar pattern[77], which may become a hallmark feature in IPF, but remains to be proven. To establish this pattern as unique to IPF will require obtaining ^{129}Xe gas exchange MRI in a well-characterized cohort

Commented [RLJ19]: R.1.7

of other conditions, such as NSIP. This condition is characterized by a homogenous inflammatory process compared to the temporal and spatially heterogeneous thickening of basement membrane that occurs with IPF. It is thus conceivable that ^{129}Xe gas exchange imaging in NSIP may reveal more homogeneously enhanced barrier uptake, coupled with both regionally enhanced and deficient RBC transfer. Moreover, preliminary evidence suggests some pulmonary vascular disease also presents with enhanced barrier and reduced RBC:barrier ratios, and thus must also be distinguished[60,79]. It is possible that such discrimination will require the development of additional biomarkers, such as dynamic ^{129}Xe spectroscopy to distinguish gas exchange impairment caused by interstitial versus pulmonary vascular conditions[80]. Ultimately, if studies can demonstrate the unique ability to identify IPF and patients who can definitively benefit from antifibrotic therapies at earlier time points, patient outcomes could be improved by confidently initiating treatment at the earliest possible time, when therapy is most likely to successfully slow progression of disease[81].

Commented [RLJ20]: R.1.8

Equally important to diagnosis is to the ability to provide prognostic information that can guide patient care. While HRCT structural imaging can be critical in establishing a diagnosis, it has proven less reliable in assessing the stage of the disease course[82]. Here ^{129}Xe MRI ultimately has the potential to provide additional prognostic benefit. For example, some patients may present late in the disease course where expensive treatment is unlikely to provide clinical benefit. ^{129}Xe MRI could be used to functionally evaluate patients, determining how much salvageable lung is present (i.e. what fraction of the lung exhibits preserved RBC transfer). By contrast, with patients exhibiting end stage fibrosis with >50% loss of RBC transfer, the ability to slow disease progression is likely diminished, and these patients may need to be listed for transplant immediately. Preliminary evidence for such a potential pattern has been recently presented by Tighe and co-workers[83]. It is conceivable that it's precisely these patients who are also at increased risk of exacerbation, another vexing prognostic problem in IPF[84]. Alternatively, patients

exhibiting a high degree of barrier uptake, but with RBC transfer that is largely preserved, may be those most likely to benefit from novel therapies. Of course, establishing ^{129}Xe MRI to facilitate such clinical decision making requires conducting prospective multi-center trials evaluating the clinical outcomes of patients categorized in this manner. An example of such a study design in other imaging contexts may be found in the PLUS trial for FDG-PET, which allowed this modality to be translated from limited academic use to becoming standard of care in patients with lung cancer being considered for surgical resection[85].

Commented [RLJ21]: R.1.9

Once therapy has been initiated for patients with IPF, there is no consensus regarding how they should be monitored[86]. Currently, a decline greater than or equal to 10% of FVC or greater than or equal to 15% of the DLco are accepted definitions of the indication of disease progression. Unfortunately, some studies have shown better than expected survival in patients with FVC losses greater than 10%, while others have demonstrated a poor prognosis even in the setting of stable FVC[87]. Although efforts are currently underway to use HRCT for quantitative assessment of reticulation, traction bronchiectasis, and honeycombing to evaluate IPF progression[88], none have seen widespread clinical use. By contrast, given its strong connection to physiology, coupled with spatially resolved functional assessment, ^{129}Xe MRI could provide added benefit in assessing treatment efficacy in individual patients. One potential paradigm would focus on assessment of barrier uptake prior to starting therapy and re-evaluating at 3 months after therapy. If microscopic barrier tissue thickening has indeed been brought under control, one might expect to detect stable or decreasing barrier uptake, coupled with stable or even improving RBC transfer. If, by contrast, barrier uptake continues to enhance, and RBC transfer defects begin to encompass a larger percentage of lung volume, it would likely indicate that treatment should be altered or stopped. Once again, such hypotheses must be bolstered by multi-center trials that ultimately

demonstrate that imaging confers patient benefit. However, with the extraordinary cost of new drugs and the burden on patients and their families, such studies should be welcomed.

Technical Development and Future Advancements

Hyperpolarized ^{129}Xe gas exchange MRI is a relatively new and rapidly evolving technique. Like any such modality, its clinical value is likely to be further enhanced by continued technical optimization and advancement, both of which will improve performance and facilitate broader dissemination. Although HP ^{129}Xe MRI appears robust and delivers isotropic voxels of $(0.3\ cm)^3$ with reasonable signal-to-noise ratios[66,89], numerous potential advancements are on the horizon. As one example, the short T2* of ^{129}Xe in the dissolved compartments has led to gas exchange imaging having been deployed primarily on 1.5 T MRI platforms. However, most major commercial MRI vendors are moving their multi-nuclear capabilities (required for ^{129}Xe MRI) to their 3.0 T platforms. To this end, Z. Wang et al recently demonstrated that the 1-point Dixon method of encoding gas exchange can be effectively deployed at 3 Telsa[66], despite the T2* of ^{129}Xe in RBCs being only ~1.1ms. This was achieved by using a short (0.69ms) selective excitation pulse, to enable imaging with TE <0.5 ms, and a read-out time matching T2* to successfully resolve and quantify ^{129}Xe in all 3 compartments[66].

In fact, it remains a significant challenge to selectively excite and image ^{129}Xe in the dissolved phase signal without also exciting the much larger (~50-100x) reservoir of gas-phase ^{129}Xe in the alveolar spaces. This often requires careful design and calibration of the RF excitation pulse to identify a narrow range of pulse durations where off-resonance excitation is minimized[90]. However, such operating points may differ across scanner platforms, RF amplifiers, and vendors. As an elegant alternative, Hahn et al have recently demonstrated a dual-echo technique that may obviate this problem entirely. Their approach exploits the much longer T2* of gas-phase vs dissolved phase ^{129}Xe such that the second echo contains only gas-phase ^{129}Xe signal[91]. This method thus removes the requirement of selectively exciting

and separately encoding the gas and dissolved phases, instead permitting all 3 compartments to be acquired simultaneously. In this approach, the 2nd, longer echo time, consists almost entirely of off-resonance gas-phase signal, which may be simply demodulated and reconstructed as the ventilation image. With suitable correction, its contaminating effect can be removed from the short-echo image, to leave only the dissolved components that can be separated by the 1-point Dixon method. By no longer requiring interleaved acquisition of gas and dissolved views, this approach could lead to even shorter breath-holds and higher spatial resolution.

A valuable next step for quantitative regional assessment of gas exchange imaging is to combine the spatial specificity of imaging with the added dynamic information available by imaging gas uptake at different diffusive uptake times used in the CSSR method[92]. This could permit such parameters as septal thickness to be quantified regionally. Such methods will benefit from development of novel multi-channel coil architectures parallel imaging acceleration methods. Moreover, while Dixon-type acquisitions provide an efficient way to image barrier uptake and RBC transfer, chemical shift imaging may provide a promising alternative to fully characterize ^{129}Xe spectral parameters such as the RBC frequency shift to provide locally resolved tissue oxygenation[93].

Several additional areas need to be addressed that span the clinical and technical domains. As described herein, the imaging patterns observed by ^{129}Xe gas exchange MRI are significantly more straightforward to interpret and quantify when they undergo quantitative binning using reference distributions derived from a healthy cohort. However, to date those reference distributions have been primarily derived from healthy young volunteers, and it is not yet known how normal aging may affect them. Moreover, such an approach and its associated reference populations will depend somewhat on choice of echo time, flip angle, repetition time, and the number of k-space views encoded and thus a consensus protocol should be quickly established and used going forward. With image acquisition protocols agreed, reference

cohorts can be recruited across centers and potentially grouped by decade to test the degree to which gas exchange patterns evolve as a part of normal aging. Moreover, although early spectroscopic studies have demonstrated encouraging initial evidence of repeatability, this work should be extended using imaging biomarkers and conducted across multiple centers to move from repeatability to reproducibility. With this information in hand, it becomes possible to begin establishing the magnitude of change in ^{129}Xe biomarkers that are clinically significant. An example of such a minimal clinically important difference (MCID) has recently been established for ^{3}He ventilation MRI in the context of asthma[94]. This work demonstrated that changes in ventilated volume as small as 110ml or 2% are clinically important. Ultimately, such studies would need to be conducted not only for ^{129}Xe ventilation, but also for its associated markers of barrier uptake and RBC transfer.

Conclusion

Hyperpolarized ^{129}Xe imaging with MRI is a powerful, emerging technique that shows promise in positively impacting the management of idiopathic pulmonary fibrosis. While multi-center clinical studies and technical validation are still needed, the method's fundamental grounding in physiology and sensitivity to micron-scale changes in blood gas barrier thickness provide a sound basis for it to ultimately positively impact the way IPF is diagnosed, staged, and treated. Just as the introduction of 3D structural imaging such as HRCT and MRI have revolutionized the ability to peer into human lung anatomy non-invasively, the addition of 3D imaging with HP ^{129}Xe MRI may now permit us to peer into its function. Thus, studies such as the seminal work of Agusti et al to characterize gas exchange impairment in IPF that once required a laboratory full of physiologists and a cadre of dedicated patients tolerating invasive exams[95], might in the future be done for every patient, using only a single inhalation of hyperpolarized ^{129}Xe.

Commented [RLJ22]: R.1.10

Commented [RLJ23]: R.1.11

Acknowledgements

Grant Support: NIH/NHLBI R01 HL105643 and NIH/NHLBI R01HL126771

Figures

*Figure 1: Different clinical trajectories in idiopathic pulmonary fibrosis (IPF). Disease begins with a subclinical period in which only radiographic findings of disease may be present, followed by a symptomatic period consisting of both pre-diagnosis and post-diagnosis clinical phases. The rate of decline and progression to death may be rapid (line A), slow (lines C and D), or mixed (curve B), with periods of relative stability interposed with periods of acute decline (star). (Figure reprinted with permission of the American Thoracic Society. Copyright © 2018 American Thoracic Society. Ley, B., Collard, H. R. & King, T. E. Clinical Course and Prediction of Survival in Idiopathic Pulmonary Fibrosis. 2011 Am. J. Respir. Crit. Care Med. **183**, 431–440. The American Journal of Respiratory and Critical Care Medicine is an official journal of the American Thoracic Society)*

*Figure 2: Axial and sagittal reformats of HRCT (**a**) compared to 3D UTE (**b**), and 3D radial image acquired at longer echo time (TE = 2.1 ms). The HRCT is acquired during breath-hold, while the MRI scans were acquired over 5.5 min of free-breathing. Fibrosis patterns and extent are well appreciated on UTE and follow what is seen on HRCT. However, at the longer 2.1 ms echo time these patterns are no longer well visualized on MRI. Nonetheless, HRCT images exhibit substantially higher spatial resolution and reduced respiratory motion. (Images reprinted courtesy of Johnson et al, Optimized 3D ultrashort echo time pulmonary MRI. Magn. Reson. Med. **70**, 1241-1250 (2013) Copyright ©1999-2018 John Wiley & sons, Inc. All rights reserved*

*Figure 3: ^{129}Xe ventilation MRI reveals heterogeneity associated with traction bronchiectasis**.** Evidence of high signal intensity in lower lobe airways, bilaterally in A and within the right lower lobe in B. These findings relate to regions of traction bronchiectasis seen on the associated computed tomography scan. (Reprinted from Nick Weatherley PhD thesis University of Sheffield 2018)*

Figure 4: Microstructural changes in IPF revealed with hyperpolarized ^{129}Xe apparent diffusion coefficient images. Honeycomb cysts (red arrow) and traction bronchiectasis (white arrows) are evident by virtue of their elevated apparent diffusion coefficient (ADC), reflective of airspace enlargement and enhanced ^{129}Xe mobility. The location of these abnormalities is consistent with findings on CT imaging. (Images courtesy of the University of Sheffield)

*Figure 5: ^{129}Xe magnetic resonance spectrum showing signal intensity in human lungs[61]. (A) NMR spectrum obtained when exciting the gas- and dissolved-phase ^{129}Xe equally, showing that the dissolved phase ^{129}Xe signal is only 1-2% as large as gas; (B) When the dissolved phase is selectively excited the barrier and RBC spectral peaks are better appreciated. (Figure reprinted from Cleveland et al, Hyperpolarized ^{129}Xe MR imaging of alveolar gas uptake in humans. PLoS One, **5**. 1-8 (2010)*

Figure 6: The first 3D images of dissolved-phase xenon in human lungs. (A) Select, 15-mm-thick slices of the 3D dissolved-phase ^{129}Xe image, left-to-right showing anterior-to-posterior cuts; (B) Geometrically corresponding 15-mm-thick slices of the 3D gas-phase HP ^{129}Xe image in the same volunteer; (C) Dissolved-phase in color, overlaid on the grayscale

*ventilation image. (Figure reprinted from Cleveland et al, Hyperpolarized ^{129}Xe MR imaging of alveolar gas uptake in humans. PLoS One, **5**. 1-8 (2010)*

*Figure 7: Quantitative ^{129}Xe spectroscopy applied to patients with idiopathic pulmonary fibrosis in a study by Kaushik et al[67]. (A) Dissolved-phase ^{129}Xe spectrum showing greatly reduced ^{129}Xe transfer to the RBC phases in patients with IPF; (B) This was quantified by the RBC:barrier ratio, for which the average in IPF subjects was 0.16 +/- 0.03, compared to 0.55 +/- 0.13 in healthy volunteers (P=0.0002). (Figure reprinted from Kaushik et al, Measuring diffusion limitation with a perfusion-limited gas-Hyperpolarized 129Xe gas-transfer spectroscopy in patients with idiopathic pulmonary fibrosis. J. Appl. Physiol. **117**, 577-585 (2014)*

Figure 8: Representative coronal gas, tissue (barrier) uptake, and RBC transfer images acquired in a healthy subject using radial hierarchical IDEAL strategy. The RBC image exhibits signal from the lung parenchyma as well as the left ventricle of the heart. (Figure reprinted from Qing et al, Regional mapping of gas uptake by blood and tissue in the human lung using hyperpolarized Xenon-129 MRI. J Magn. Reson. Imag. 2014)

*Figure 9: HP ^{129}Xe gas exchange images comparing healthy volunteers to patients with IPF acquired using the 1-point Dixon method. Compared to healthy volunteers, ^{129}Xe transfer to RBCs could be seen to be focally impaired in base and periphery of the lungs of patients with IPF. (Reprinted from Kaushik et al, Single-breath clinical imaging of hyperpolarized 129Xe in the airspaces, barrier, and red blood cells using an interleaved 3D radial 1-point Dixon acquisition. Magn. Reson. Med. **75**, 1434-1443 (2016)*

*Figure 10: Healthy reference distributions proposed for ^{129}Xe ventilation, barrier uptake, and RBC transfer. These data were generated from 10 healthy volunteer subjects and color bins were assigned based on a Gaussian curve fit, with each bin being assigned a width that is one standard deviation of the reference distribution. In this way normal compartments are defined as lying within one standard deviation of the reference mean (green), while "defects" are those 2 standard deviations below the mean and high barrier uptake values are represented in pink and purple colors. (Image reprinted from Wang et al, Quantitative analysis of hyperpolarized ^{129}Xe gas transfer MRI. Med Phys **44**, 2415-2429 (2017)*

*Figure 11: Representative healthy [left] and IPF [right] subjects and the corresponding quantitative color maps and histograms of ventilation, barrier uptake and RBC transfer. Note the high degree of barrier uptake in IPF relative to the healthy subject, coupled with focal defects in ^{129}Xe transfer to the RBCs in the lung base and periphery. (Figure reprinted from Wang et al, Quantitative analysis of hyperpolarized ^{129}Xe gas transfer MRI. Med Phys **44**, 2415-2429 (2017)*

Figure 12: With the exception of ^{129}Xe ventilation, ^{129}Xe gas exchange metrics such as barrier uptake, RBC transfer and RBC/barrier ratio all correlate well with FVC and DLCO. The correlation between RBC/barrier and DLCO (r=0.94) is particularly strong. (Figure reprinted from Wang et al, Using hyperpolarized ^{129}Xe MRI to quantify regional gas

*transfer in idiopathic pulmonary fibrosis. Thorax **73**, 21-28 (2018) Copyright ©1999-2018 John Wiley & sons, Inc. All rights reserved*

*Figure 13: Concordance and discordance between HRCT and ^{129}Xe gas exchange MRI and potential models of gas exchange[77]. In a healthy lung (A), gaseous ^{129}Xe efficiently diffuses from the alveolus, across a thin barrier to RBCs, resulting in signal intensities in the normal range for both compartments. In IPF, some regions of barrier enhancement (B, arrows) are associated with decreased RBC transfer (diffusion block). As the disease progresses (C), scarring causes ^{129}Xe to stop diffusing into or through the barrier (normal or low range), while RBC transfer is dramatically reduced. This likely represents unperfused tissue. Most interesting are regions depicting the coexistence of high barrier uptake and preserved RBC transfer (D, arrow). This may represent regions of disease activity that could be responsive to therapy. Notably many of these areas appear normal on CT. (Figure reprinted from J. Wang et al, Using hyperpolarized ^{129}Xe MRI to quantify regional gas transfer in idiopathic pulmonary fibrosis. Thorax **73**, 21-28 (2018) Copyright ©1999-2018 John Wiley & sons, Inc. All rights reserved*

Figure 14: Longitudinal changes in FVC, DLCO and ^{129}Xe spectroscopy derived RBC/TP (RBC:barrier ratio) in patients with IPF patients. Notably, the conventional metrics FVC and DLCO do not exhibit a significant change over the 12-month interval, whereas RBC:barrier shows a decreases at 6-months, which becomes statistically significant at 12 months. (Figure reprinted from Chan et al. Abstract 4353 ISMRM 2018)

Figure 15: Example of improving ^{129}Xe gas exchange metrics for a patient on current therapy. This patient started anti-fibrotic therapy one month prior to baseline MRI and presented with 49% high barrier uptake, and focal RBC transfer defects at the lung bases resulting in 35% low RBC transfer. Upon return 5 months later, the percentage of lung exhibiting high barrier uptake had decreased to 30%, while the RBC transfer defects remained stable at 35% of lung volume.

References

1. Raghu, G., Weycker, D., Edelsberg, J., Bradford, W. Z. & Oster, G. Incidence and Prevalence of Idiopathic Pulmonary Fibrosis. *Am. J. Respir. Crit. Care Med.* **174,** 810–816 (2006).

2. Demedts, M. & Costabel, U. ATS/ERS international multidisciplinary consensus classification of the idiopathic interstitial pneumonias. *Eur. Respir. J.* **19,** 794–796 (2002).

3. King, T. E. *et al.* Idiopathic Pulmonary Fibrosis: Diagnosis and Treatment. *Am. J. Respir. Crit. Care Med.* **161,** 646–664 (2000).

4. King, T. E., Pardo, A. & Selman, M. Idiopathic pulmonary fibrosis. *Lancet* **378,** 1949–1961 (2011).

5. Raghu, G. *et al.* An Official ATS/ERS/JRS/ALAT Statement: Idiopathic pulmonary fibrosis: Evidence-based guidelines for diagnosis and management. *Am. J. Respir. Crit. Care Med.* **183,** 788–824 (2011).

6. Richeldi, L. *et al.* Efficacy and Safety of Nintedanib in Idiopathic Pulmonary Fibrosis. *N. Engl. J. Med.* **370,** 2071–2082 (2014).

7. Noble, P. W. *et al.* Pirfenidone in patients with idiopathic pulmonary fibrosis (CAPACITY): Two randomised trials. *Lancet* **377,** 1760–1769 (2011).

8. Karimi-Shah, B. A. & Chowdhury, B. A. Forced Vital Capacity in Idiopathic Pulmonary Fibrosis — FDA Review of Pirfenidone and Nintedanib. *N. Engl. J. Med.* **372,** 1189–1191 (2015).

9. King, T. E. *et al.* A Phase 3 Trial of Pirfenidone in Patients with Idiopathic Pulmonary Fibrosis. *N. Engl. J. Med.* **370,** 2083–2092 (2014).

10. Martinez, F. J. *et al.* Idiopathic pulmonary fibrosis. *Nat. Rev. Dis. Prim.* **3,** 17074 (2017).

11. Aryal, S. & Nathan, S. D. An update on emerging drugs for the treatment of idiopathic pulmonary fibrosis. *Expert Opin. Emerg. Drugs* **In Press,** (2018).

12. Austrian, R. *et al.* Clinical and physiologic features of some types of pulmonary diseases with impairment of alveolar-capillary diffusion. *Am. J. Med.* **11,** 667–685 (1951).

13. Plantier, L. *et al.* Physiology of the lung in idiopathic pulmonary fibrosis. *Eur. Respir. Rev.* **27,** 170062 (2018).

14. Cottin, V. Combined pulmonary fibrosis and emphysema: a distinct underrecognised entity. *Eur. Respir. J.* **26,** 586–593 (2005).

15. Mejía, M. *et al.* Idiopathic Pulmonary Fibrosis and Emphysema. *Chest* **136,** 10–15 (2009).

16. Ryerson, C. J. *et al.* Clinical Features and Outcomes in Combined Pulmonary Fibrosis and Emphysema in Idiopathic Pulmonary Fibrosis. *Chest* **144,** 234–240 (2013).

17. Lynch, D. A. *et al.* Diagnostic criteria for idiopathic pulmonary fibrosis: a Fleischner Society White Paper. *Lancet Respir. Med.* **6,** 138–153 (2018).

18. Kaarteenaho, R. The current position of surgical lung biopsy in the diagnosis of idiopathic pulmonary fibrosis. *Respir. Res.* **14,** 43 (2013).

19. Huie, T. J. & Brown, K. K. Definitions of disease: Should possible and probable idiopathic pulmonary fibrosis be enrolled in treatment trials? *Respir. Investig.* **53,** 88–92 (2015).

20. Copley, S. J. *et al.* Lung Morphology in the Elderly: Comparative CT Study of Subjects over 75 Years Old versus Those under 55 Years Old. *Radiology* **251,** 566–573 (2009).

21. Ley, B., Collard, H. R. & King, T. E. Clinical Course and Prediction of Survival in Idiopathic Pulmonary Fibrosis. *Am. J. Respir. Crit. Care Med.* **183,** 431–440 (2011).

22. Nathan, S. D. *et al.* Long-term Course and Prognosis of Idiopathic Pulmonary Fibrosis in the New Millennium. *Chest* **140,** 221–229 (2011).

23. Jensen, R. L. *et al.* Instrument accuracy and reproducibility in measurements of pulmonary function. *Chest* **132,** 388–395 (2007).

24. Du Bois, R. M. *et al.* Forced vital capacity in patients with idiopathic pulmonary fibrosis: Test properties and minimal clinically important difference. *Am. J. Respir. Crit. Care Med.* **184,** 1382–1389 (2011).

25. Yamauchi, H. *et al.* Clinical Course and Changes in High-Resolution Computed Tomography Findings in Patients with Idiopathic Pulmonary Fibrosis without Honeycombing. *PLoS One* **11,** e0166168 (2016).

26. Lee, H. Y. *et al.* High-Resolution CT Findings in Fibrotic Idiopathic Interstitial Pneumonias With Little Honeycombing: Serial Changes and Prognostic Implications. *Am. J. Roentgenol.* **199,** 982–989 (2012).

27. Hwang, J.-H. *et al.* Longitudinal Follow-up of Fibrosing Interstitial Pneumonia. *J. Thorac. Imaging* **26,** 209–217 (2011).

28. Oda, K. *et al.* High-resolution CT scoring system-based grading scale predicts the clinical outcomes in patients with idiopathic pulmonary fibrosis. *Respir. Res.* **15,** 10 (2014).

29. Robbie, H., Daccord, C., Chua, F. & Devaraj, A. Evaluating disease severity in idiopathic pulmonary fibrosis. *Eur. Respir. Rev.* **26,** 170051 (2017).

30. Hansell, D. M. *et al.* CT staging and monitoring of fibrotic interstitial lung diseases in clinical practice and treatment trials: a Position Paper from the Fleischner society. *Lancet Respir. Med.* **3,** 483–496 (2015).

31. Sverzellati, N. *et al.* Visual score and quantitative CT indices in pulmonary fibrosis: Relationship with physiologic impairment. *Radiol. Med.* **112,** 1160–1172 (2007).

32. Maldonado, F. *et al.* Automated quantification of radiological patterns predicts survival in idiopathic pulmonary fibrosis. *Eur. Respir. J.* **43,** 204–212 (2014).

33. Jacob, J. *et al.* Predicting Outcomes in Idiopathic Pulmonary Fibrosis Using Automated CT Analysis. *Am. J. Respir. Crit. Care Med.* **In Press,** (2018).

34. Johnson, K. M., Fain, S. B., Schiebler, M. L. & Nagle, S. Optimized 3D ultrashort echo time pulmonary MRI. *Magn. Reson. Med.* **70,** 1241–1250 (2013).

35. Wild, J. M. Imaging pathophysiological changes in the lungs in IPF with xenon magnetic resonance imaging. *Thorax* **73,** 1–1 (2018).

36. Ebner, L. *et al.* The role of hyperpolarized 129 xenon in MR imaging of pulmonary function. *Eur. J. Radiol.* **86,** 343–352 (2017).

37. Kern, A. L. & Vogel-Claussen, J. Hyperpolarized gas MRI in pulmonology. *Br. J. Radiol.* 20170647 (2018). doi:10.1259/bjr.20170647

38. Kirby, M. *et al.* Hyperpolarized 3 He and 129 Xe MR Imaging in Healthy Volunteers and Patients with Chronic Obstructive Pulmonary Disease. *Radiology* **265,** 600–610 (2012).

39. Svenningsen, S. *et al.* What are ventilation defects in asthma? *Thorax* **69,** 63–71 (2014).

40. Parraga, G. *et al.* Hyperpolarized 3He Ventilation Defects and Apparent Diffusion Coefficients in Chronic Obstructive Pulmonary Disease. *Invest. Radiol.* **42,** 384–391 (2007).

41. Salerno, M. *et al.* Emphysema: Hyperpolarized Helium 3 Diffusion MR Imaging of the Lungs Compared with Spirometric Indexes—Initial Experience. *Radiology* **222,** 252–260 (2002).

42. Svenningsen, S. *et al.* Sputum Eosinophilia and Magnetic Resonance Imaging Ventilation Heterogeneity in Severe Asthma. *Am. J. Respir. Crit. Care Med.* **197,** 876–884 (2018).

43. Altes, T. A. *et al.* Use of hyperpolarized helium-3 MRI to assess response to ivacaftor treatment in patients with cystic fibrosis. *J. Cyst. Fibros.* **16,** 267–274 (2017).

44. He, M. *et al.* Dose and pulse sequence considerations for hyperpolarized 129Xe ventilation MRI. *Magn. Reson. Imaging* **33,** 877–885 (2015).

45. Diaz, S. *et al.* Validity of apparent diffusion coefficient hyperpolarized 3He-MRI using MSCT and pulmonary function tests as references. *Eur. J. Radiol.* **71,** 257–263 (2009).

46. Driehuys, B. *et al.* Chronic Obstructive Pulmonary Disease: Safety and Tolerability of

Hyperpolarized 129 Xe MR Imaging in Healthy Volunteers and Patients. *Radiology* **262,** 279–289 (2012).

47. Shukla, Y. *et al.* Hyperpolarized 129Xe Magnetic Resonance Imaging. *Acad. Radiol.* **19,** 941–951 (2012).

48. Walkup, L. L. *et al.* Feasibility, tolerability and safety of pediatric hyperpolarized 129Xe magnetic resonance imaging in healthy volunteers and children with cystic fibrosis. *Pediatr. Radiol.* **46,** 1651–1662 (2016).

49. Xu, X. *et al.* Hyperpolarized 129 Xe gas lung MRI-SNR and T 2 * comparisons at 1.5 T and 3 T. *Magn. Reson. Med.* **68,** 1900–1904 (2012).

50. Dregely, I. *et al.* 32-channel phased-array receive with asymmetric birdcage transmit coil for hyperpolarized xenon-129 lung imaging. *Magn. Reson. Med.* **70,** 576–583 (2013).

51. Rao, M., Robb, F. & Wild, J. M. Dedicated receiver array coil for 1 H lung imaging with same-breath acquisition of hyperpolarized 3 He and 129 Xe gas. *Magn. Reson. Med.* **74,** 291–299 (2015).

52. Stewart, N. J., Norquay, G., Griffiths, P. D. & Wild, J. M. Feasibility of human lung ventilation imaging using highly polarized naturally abundant xenon and optimized three-dimensional steady-state free precession. *Magn. Reson. Med.* **74,** 346–352 (2015).

53. Chan, H.-F., Stewart, N. J., Norquay, G., Collier, G. J. & Wild, J. M. 3D diffusion-weighted 129 Xe MRI for whole lung morphometry. *Magn. Reson. Med.* **79,** 2986–2995 (2018).

54. Svenningsen, S. *et al.* Hyperpolarized 3 He and 129 Xe MRI: Differences in asthma before bronchodilation. *J. Magn. Reson. Imaging* **38,** 1521–1530 (2013).

55. He, M. *et al.* Differentiating Early Stage and Later Stage IPF Using Hyperpolarized 129Xe Ventilation MRI. *Am. J. Respir. Crit. Care Med.* **193,** A6215 (2016).

56. Ouriadov, A. *et al.* Lung morphometry using hyperpolarized 129 Xe apparent diffusion coefficient anisotropy in chronic obstructive pulmonary disease. *Magn. Reson. Med.* **70,** 1699–1706 (2013).

57. Todd, N. W., Atamas, S. P., Luzina, I. G. & Galvin, J. R. Permanent alveolar collapse is the predominant mechanism in idiopathic pulmonary fibrosis. *Expert Rev. Respir. Med.* **9,** 411–418 (2015).

58. Chen, R. Y. *et al.* Tissue-blood partition coefficient for xenon: temperature and hematocrit dependence. *J. Appl. Physiol.* **49,** 178–183 (1980).

59. Roos, J. E., McAdams, H. P., Kaushik, S. S. & Driehuys, B. Hyperpolarized Gas MR Imaging. *Magn. Reson. Imaging Clin. N. Am.* **23,** 217–229 (2015).

60. Wang, Z. *et al.* Quantitative analysis of hyperpolarized 129 Xe gas transfer MRI. *Med. Phys.* **44,** 2415–2428 (2017).

61. Cleveland, Z. I. *et al.* Hyperpolarized 129Xe MR imaging of alveolar gas uptake in humans. *PLoS One* **5,** 1–8 (2010).

62. Mugler, J. P. *et al.* Simultaneous magnetic resonance imaging of ventilation distribution and gas uptake in the human lung using hyperpolarized xenon-129. *Proc. Natl. Acad. Sci.* **107,** 21707–

21712 (2010).

63. Mugler, J. P. *et al.* Image-based Measurement of T2* for Dissolved-phase Xe129 in the Human Lung. *Proc. Intl. Soc. Mag. Reson. Med* **20,** 2012 (2012).

64. Qing, K. *et al.* Regional mapping of gas uptake by blood and tissue in the human lung using hyperpolarized xenon-129 MRI. *J. Magn. Reson. Imaging* **39,** 346–359 (2014).

65. Kaushik, S. S. *et al.* Single-breath clinical imaging of hyperpolarized 129 xe in the airspaces, barrier, and red blood cells using an interleaved 3D radial 1-point Dixon acquisition. *Magn. Reson. Med.* **75,** 1434–1443 (2016).

66. Wang, Z. *et al.* Hyperpolarized 129 Xe gas transfer MRI: the transition from 1.5T to 3T. *Magn. Reson. Med.* **In Press,** (2018).

67. Kaushik, S. S. *et al.* Measuring diffusion limitation with a perfusion-limited gas--Hyperpolarized 129Xe gas-transfer spectroscopy in patients with idiopathic pulmonary fibrosis. *J. Appl. Physiol.* **117,** 577–585 (2014).

68. Robertson, S. H. *et al.* Uncovering a third dissolved-phase 129Xe resonance in the human lung: Quantifying spectroscopic features in healthy subjects and patients with idiopathic pulmonary fibrosis. *Magn. Reson. Med.* **78,** 1306–1315 (2017).

69. Cleveland, Z. I. *et al.* 3D MRI of impaired hyperpolarized 129 Xe uptake in a rat model of pulmonary fibrosis. *NMR Biomed.* **27,** 1502–1514 (2014).

70. Patz, S. *et al.* Human Pulmonary Imaging and Spectroscopy with Hyperpolarized 129Xe at 0.2T.

Acad. Radiol. **15,** 713–727 (2008).

71. Stewart, N. J. *et al.* Experimental validation of the hyperpolarized 129 Xe chemical shift saturation recovery technique in healthy volunteers and subjects with interstitial lung disease. *Magn. Reson. Med.* **74,** 196–207 (2015).

72. Stewart, N. J. *et al.* Reproducibility of quantitative indices of lung function and microstructure from 129 Xe chemical shift saturation recovery (CSSR) MR spectroscopy. *Magn. Reson. Med.* **77,** 2107–2113 (2017).

73. Driehuys, B. *et al.* Imaging alveolar-capillary gas transfer using hyperpolarized 129Xe MRI. *Proc Natl Acad Sci U S A* **103,** 18278–18283 (2006).

74. Tsao, J. & Jiang, Y. Hierarchical IDEAL: Fast, robust, and multiresolution separation of multiple chemical species from multiple echo times. *Magn. Reson. Med.* **70,** 155–159 (2013).

75. Coxson, H. O. *et al.* Quantification of Idiopathic Pulmonary Fibrosis Using Computed Tomography and Histology. *Am J Respir Crit Care Med* **155,** 1649–1656 (1997).

76. He, M., Driehuys, B., Que, L. G. & Huang, Y.-C. T. Using Hyperpolarized 129Xe MRI to Quantify the Pulmonary Ventilation Distribution. *Acad. Radiol.* **23,** 1521–1531 (2016).

77. Wang, J. M. *et al.* Using hyperpolarized 129 Xe MRI to quantify regional gas transfer in idiopathic pulmonary fibrosis. *Thorax* **73,** 21–28 (2018).

78. Chan, H.-F. *et al.* Hyperpolarized 129Xe MR spectroscopy detects short-term changes in lung gas exchange efficiency in idiopathic pulmonary fibrosis. *Proc. Intl. Soc. Mag. Reson. Med.* **26,** 0966

(2018).

79. Dahhan, T. *et al.* Abnormalities in Hyperpolarized 129 Xe Magnetic Resonance Imaging and Spectroscopy in two Patients with Pulmonary Vascular Disease. *Pulm. Circ.* **6,** 126–131 (2016).

80. Bier, E. *et al.* Quantifying Changes in Time-Resolved Hyperpolarized 129Xe Spectroscopy among Healthy Volunteers, Subjects with Idiopathic Pulmonary Fibrosis, and Subjects with Pulmonary Arterial Hypertension. in *Proceedings of the International Society of Magnetic Resonance in Medicine, 26th Annual Meeting* #4476 (2018).

81. Molina-Molina, M. *et al.* Importance of early diagnosis and treatment in idiopathic pulmonary fibrosis. *Expert Rev. Respir. Med.* **12,** 537–539 (2018).

82. Gruden, J. F. CT in Idiopathic Pulmonary Fibrosis: Diagnosis and Beyond. *Am. J. Roentgenol.* **206,** 495–507 (2016).

83. Tighe, R. M. *et al.* in *A73. DIFFUSE PARENCHYMAL LUNG DISEASE: NOVEL MECHANISMS, BIOMARKERS, AND THERAPEUTICS* A2341–A2341 (American Thoracic Society, 2018). doi:doi:10.1164/ajrccm-conference.2018.197.1_MeetingAbstracts.A2341

84. Collard, H. R. *et al.* Acute Exacerbation of Idiopathic Pulmonary Fibrosis. An International Working Group Report. *Am. J. Respir. Crit. Care Med.* **194,** 265–275 (2016).

85. van Tinteren, H. *et al.* Effectiveness of positron emission tomography in the preoperative assessment of patients with suspected non-small-cell lung cancer: the PLUS multicentre randomised trial. *Lancet* **359,** 1388–1392 (2002).

86. Fernández Fabrellas, E., Peris Sánchez, R., Sabater Abad, C. & Juan Samper, G. Prognosis and Follow-Up of Idiopathic Pulmonary Fibrosis. *Med. Sci.* **6,** 51 (2018).

87. Collard, H. R. *et al.* Changes in Clinical and Physiologic Variables Predict Survival in Idiopathic Pulmonary Fibrosis. *Am. J. Respir. Crit. Care Med.* **168,** 538–542 (2003).

88. Jacob, J. *et al.* Mortality prediction in idiopathic pulmonary fibrosis: evaluation of computer-based CT analysis with conventional severity measures. *Eur. Respir. J.* **49,** 1601011 (2017).

89. Rankine, L. J. *et al.* Correlation of Regional Lung Ventilation and Gas Transfer to Red Blood Cells: Implications for Functional-Avoidance Radiation Therapy Planning. *Int. J. Radiat. Oncol.* **101,** 1113–1122 (2018).

90. Leung, G., Norquay, G., Schulte, R. F. & Wild, J. M. Radiofrequency pulse design for the selective excitation of dissolved 129 Xe. *Magn. Reson. Med.* **73,** 21–30 (2015).

91. Hahn, A. D., Kammerman, J. & Fain, S. B. Removal of hyperpolarized 129 Xe gas-phase contamination in spectroscopic imaging of the lungs. *Magn. Reson. Med.* (2018). doi:10.1002/mrm.27349

92. Stewart, N. J. & Wild, J. M. Integrated Spectroscopic Imaging (CSI) and Chemical Shift Saturation Recovery (CSSR) of Hyperpolarized 129Xe in the Human Lungs. *Proc. Intl. Soc. Mag. Reson.* **23,** 1485 (2015).

93. Mata, J. *et al.* Evaluation of Regional Lung Function in Interstitial Lung Disease with Hyperpolarized Xenon-129 Lung 3D SB-CSI. *ISMRM Annu. Meet.* 4901 (2017).

94. Eddy, R. L., Svenningsen, S., McCormack, D. G. & Parraga, G. What is the minimal clinically important difference for helium-3 magnetic resonance imaging ventilation defects? *Eur. Respir. J.* **51,** 1800324 (2018).

95. Agustí, A. G. N. *et al.* Mechanisms of Gas-exchange Impairment in Idiopathic Pulmonary Fibrosis. *Am. Rev. Respir. Dis.* **143,** 219–225 (1991).

Figure 1

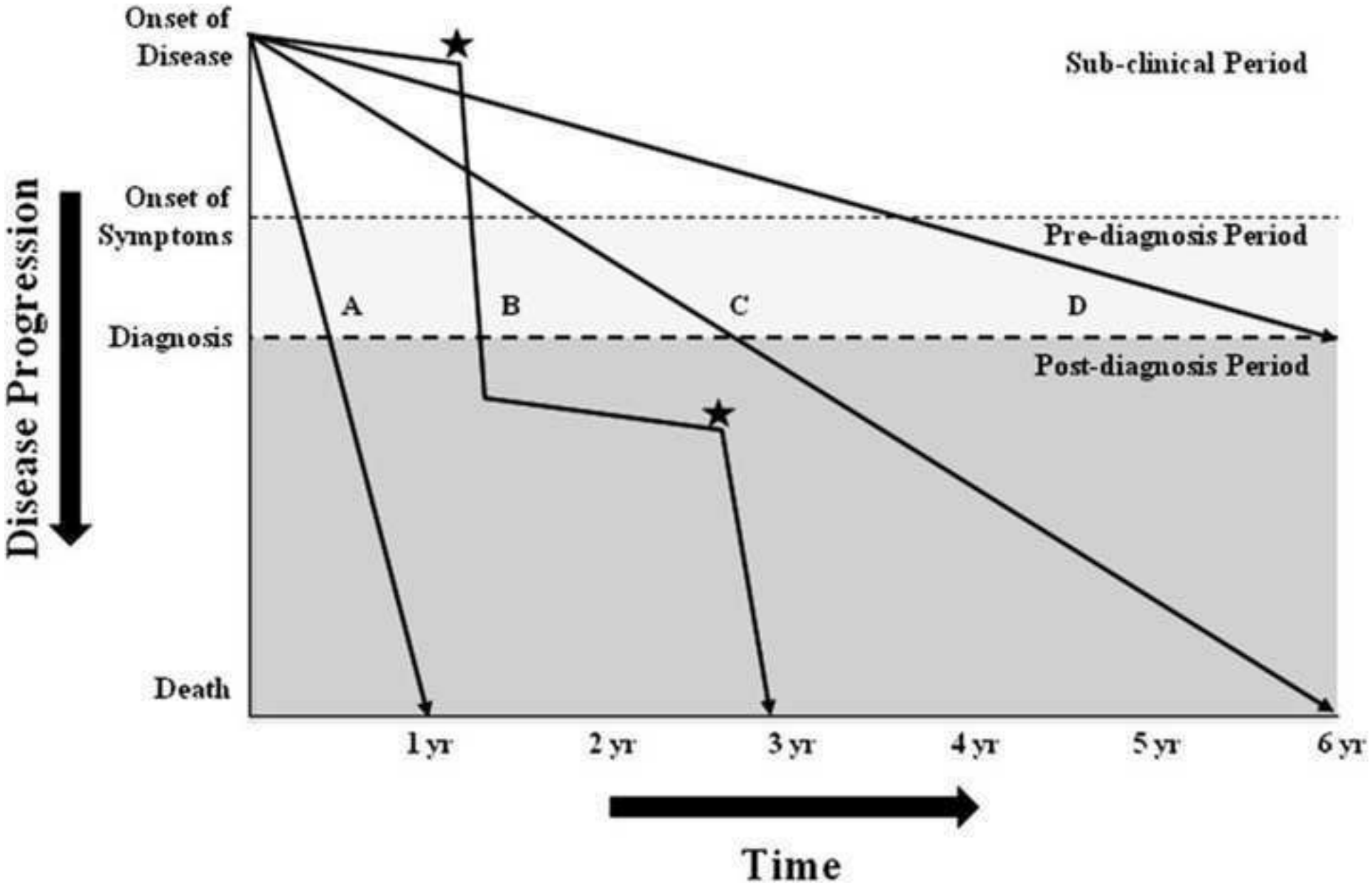

Figure 2

Click here to access/download;Figure;Figure2.jpg

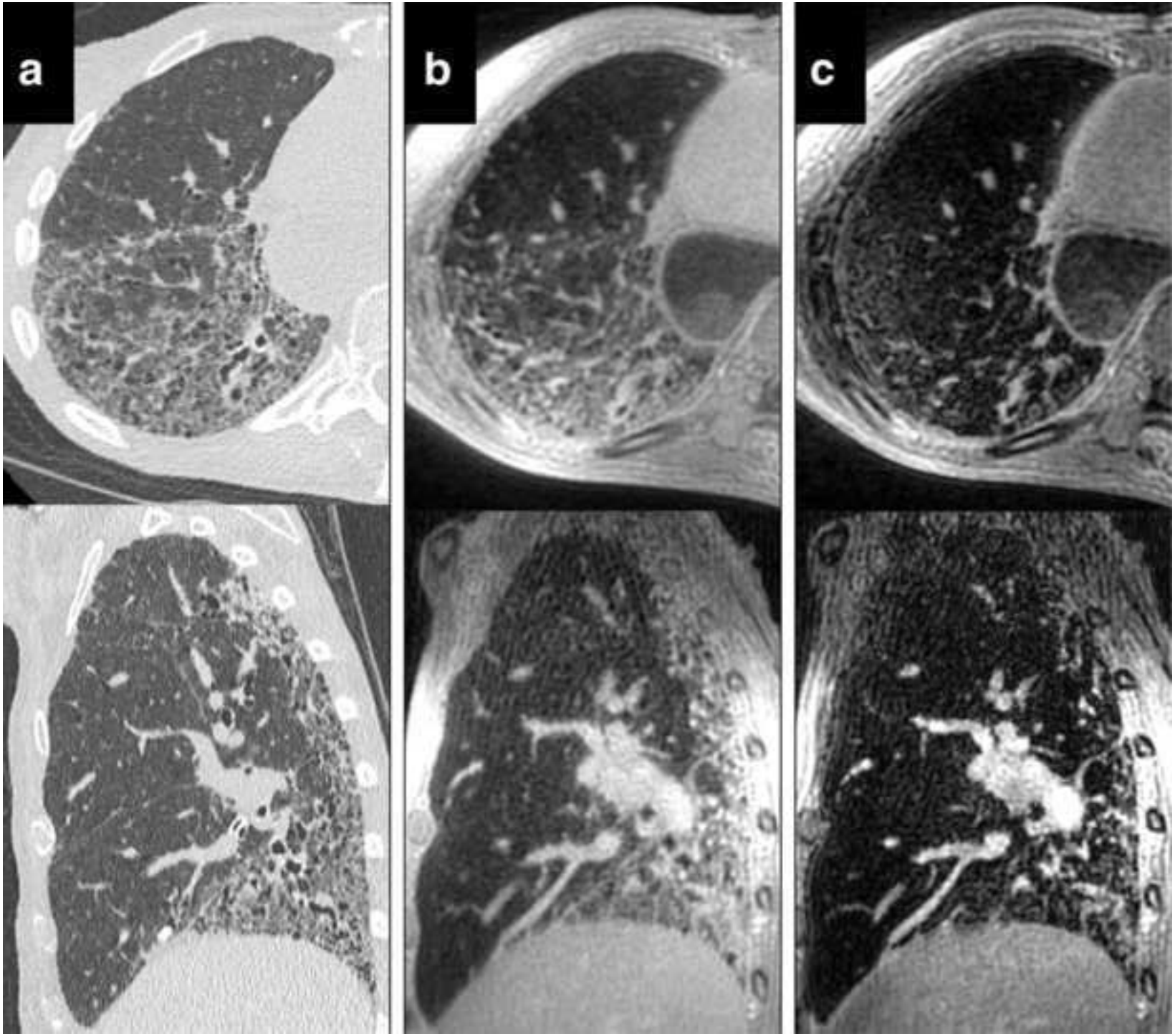

Figure 3

Click here to access/download;Figure;Figure3.png

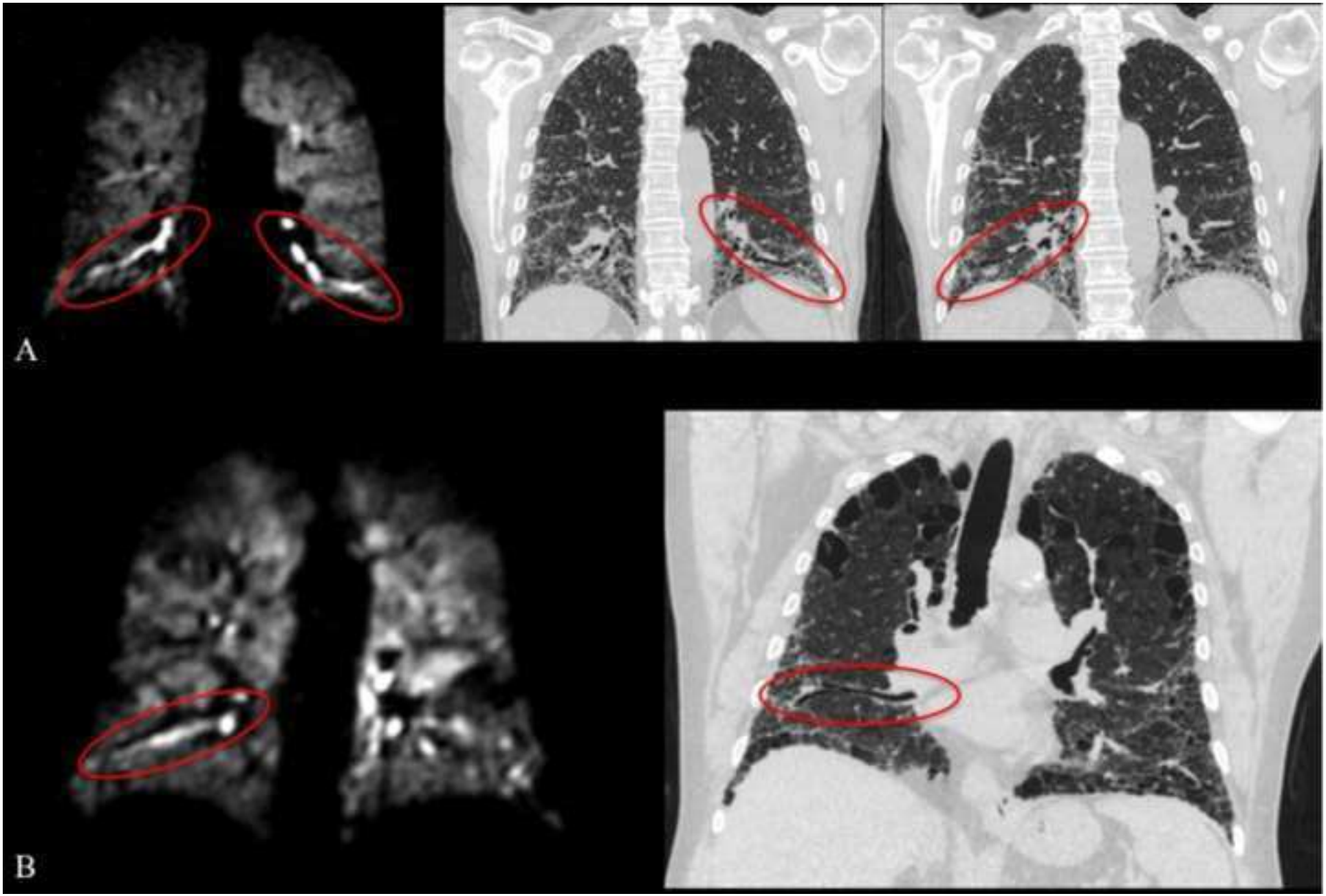

Figure 4

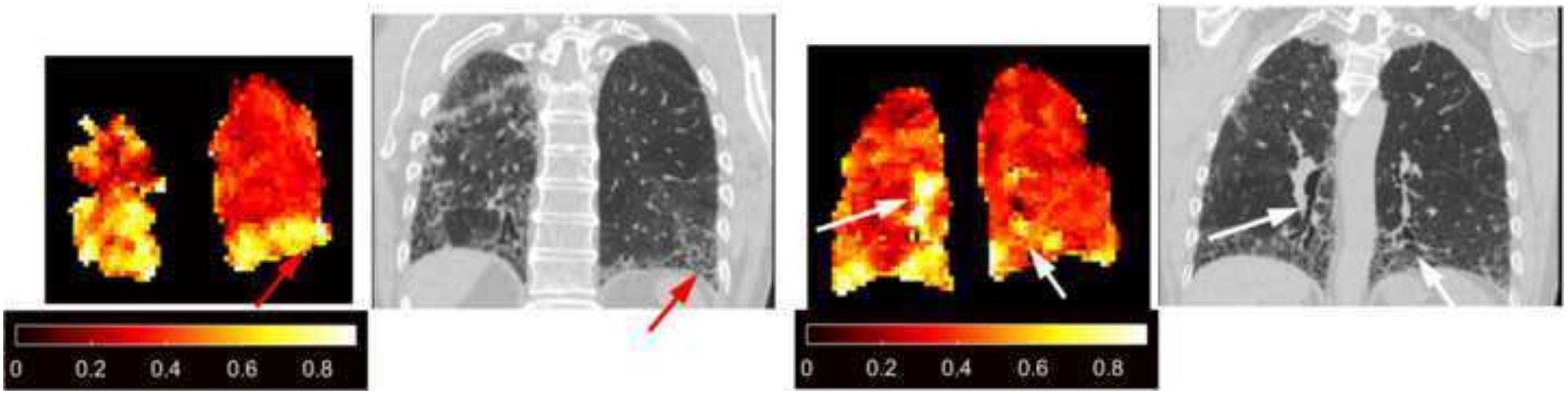

Figure 5

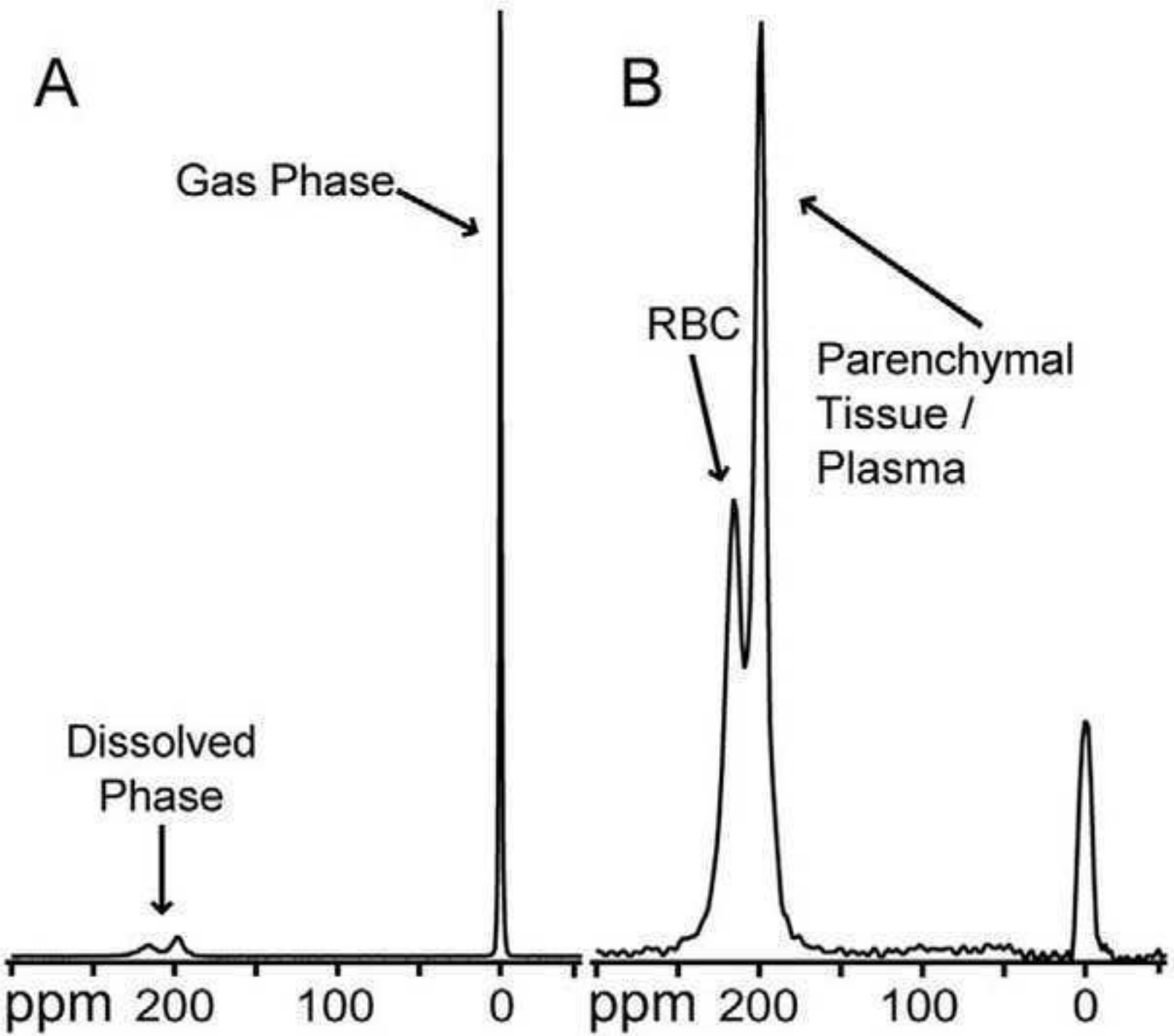

Figure 6

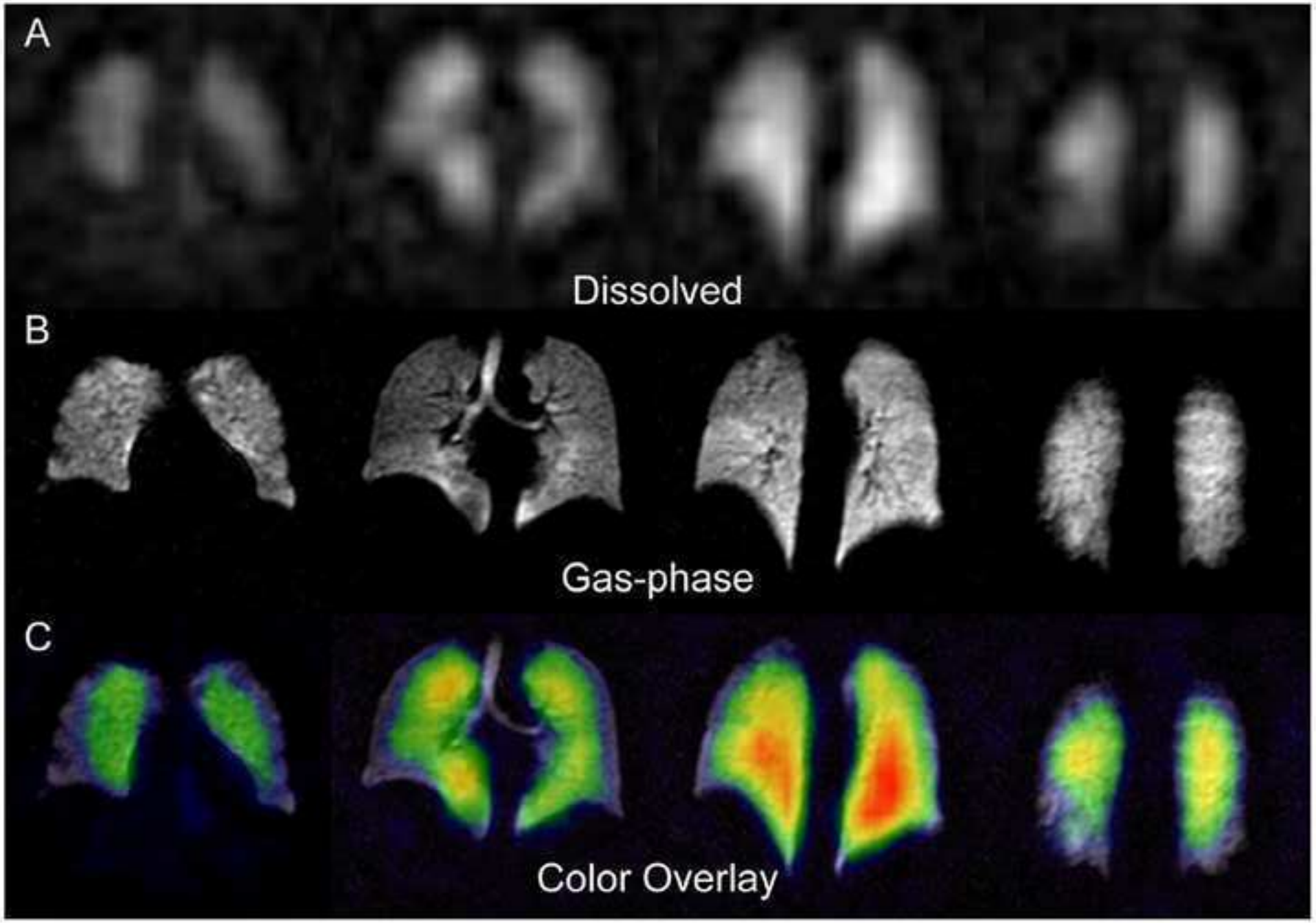

Figure 7

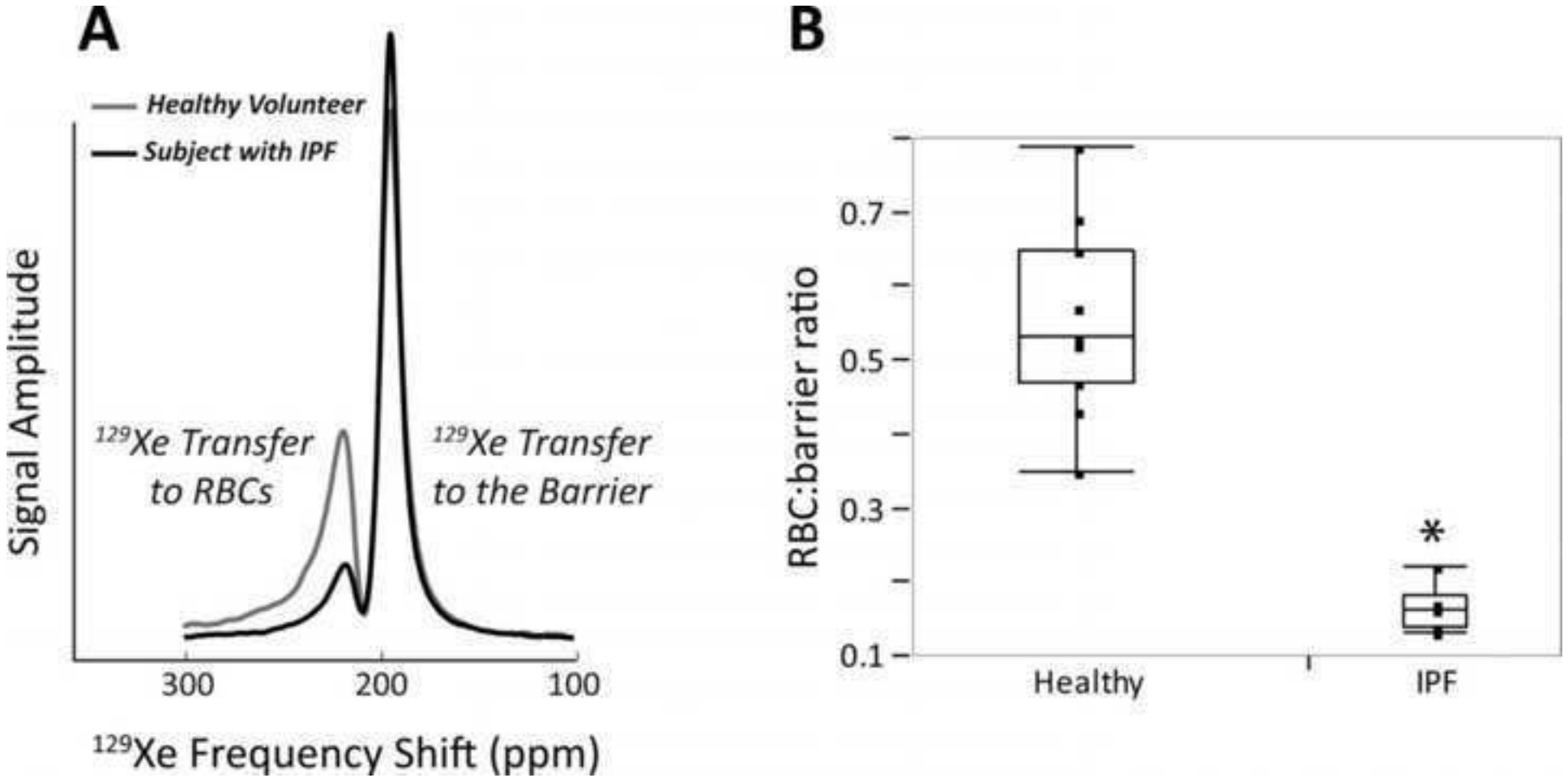

Figure 8

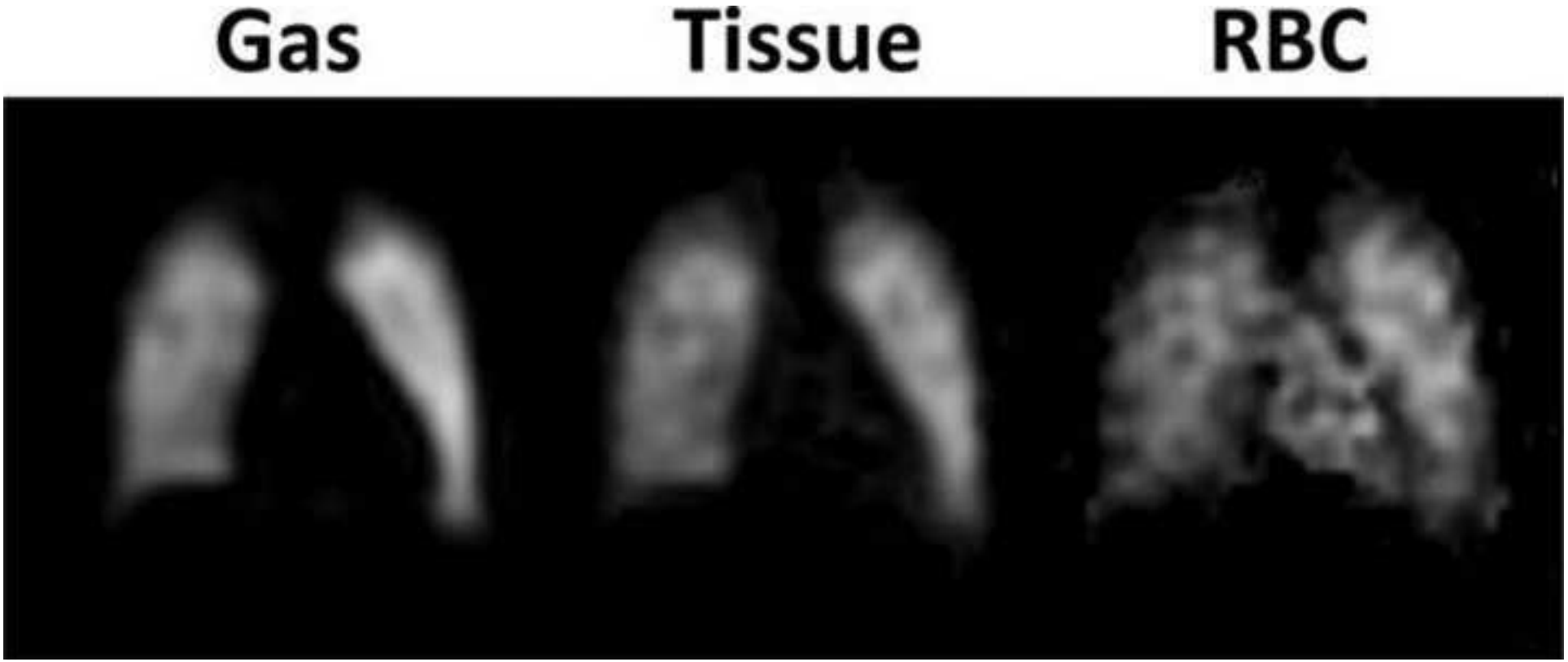

Figure 9

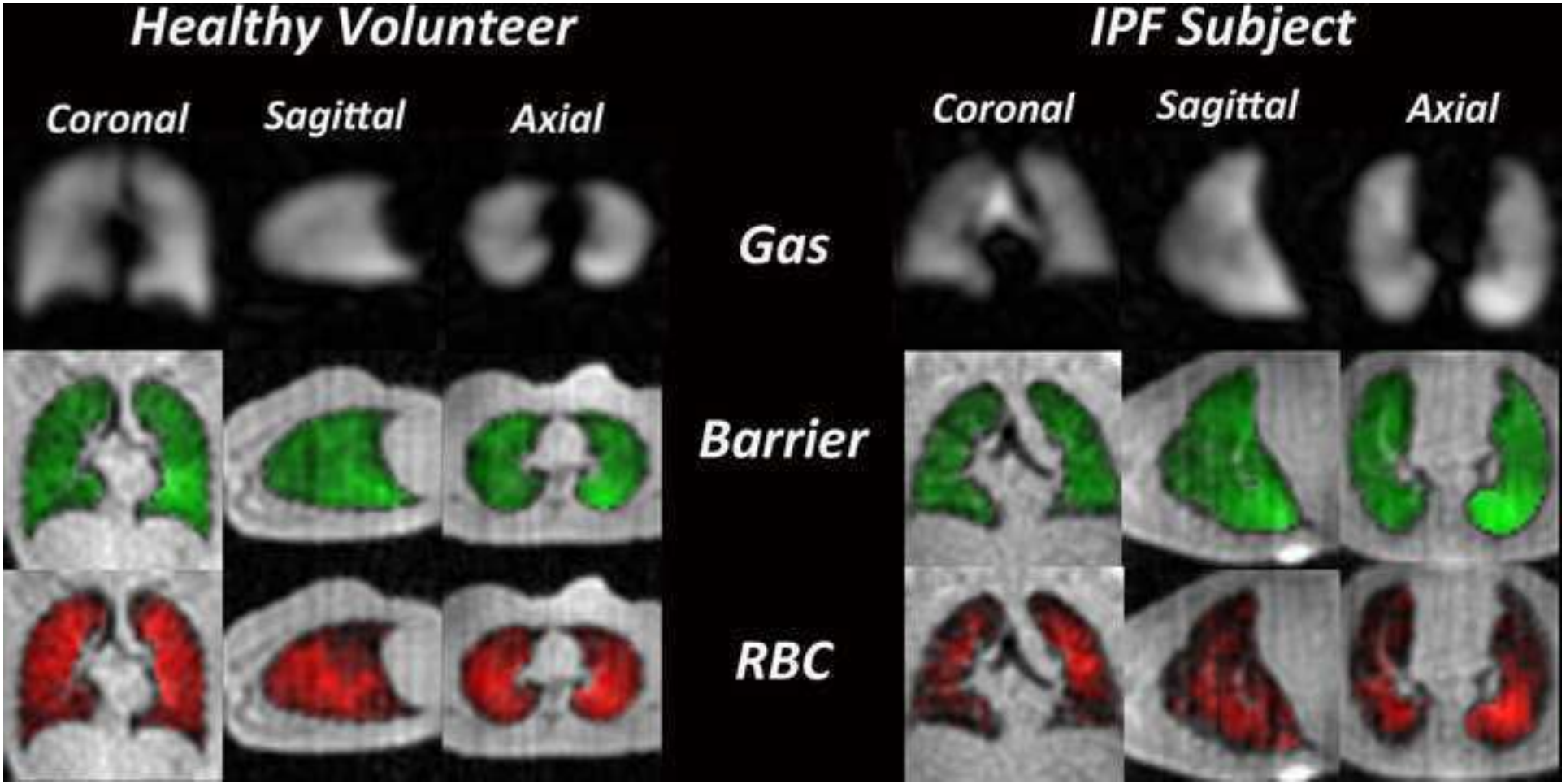

Figure 10

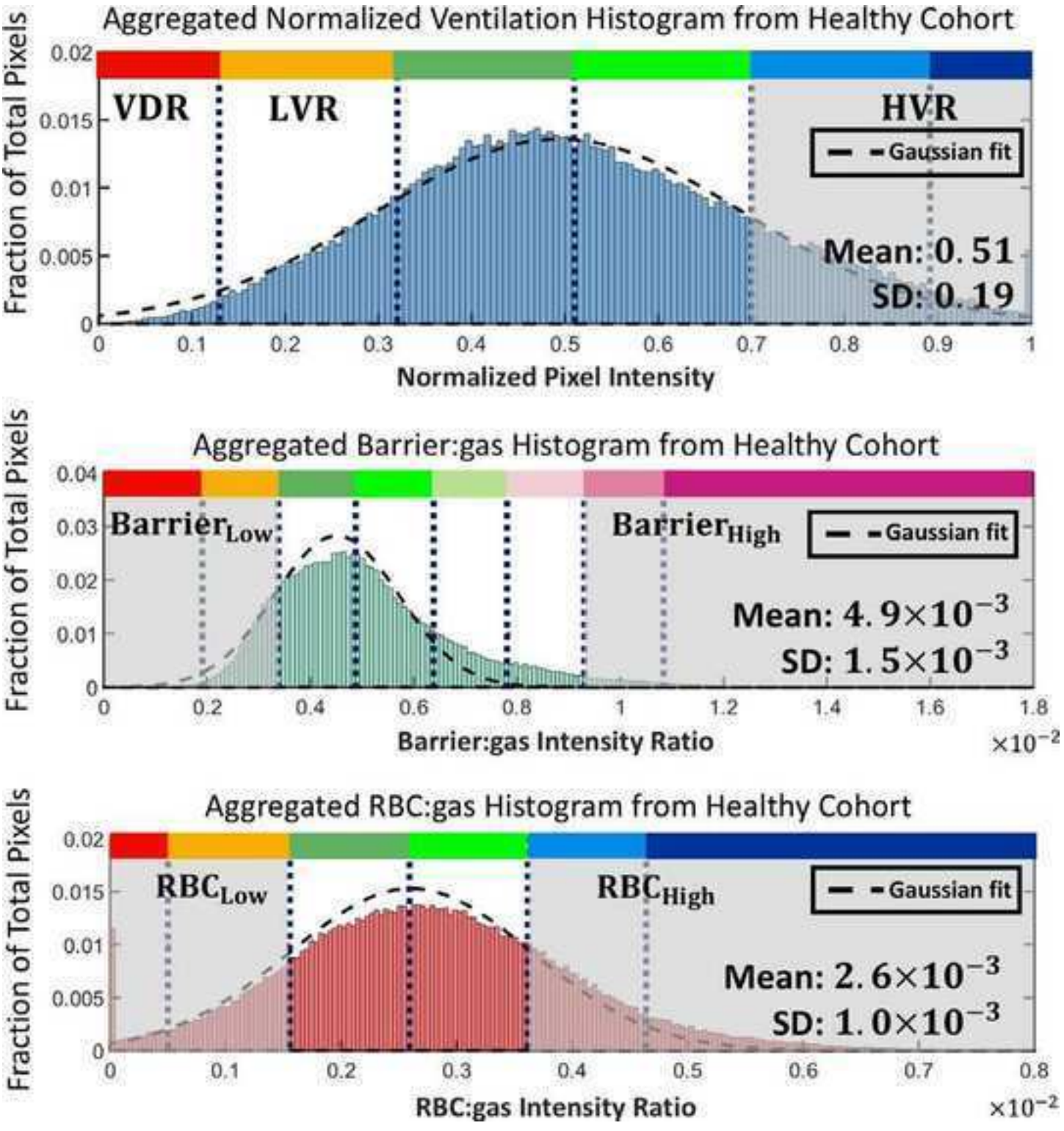

Figure 11 (left)

Click here to access/download;Figure;Figure new11_LEFT.jpg

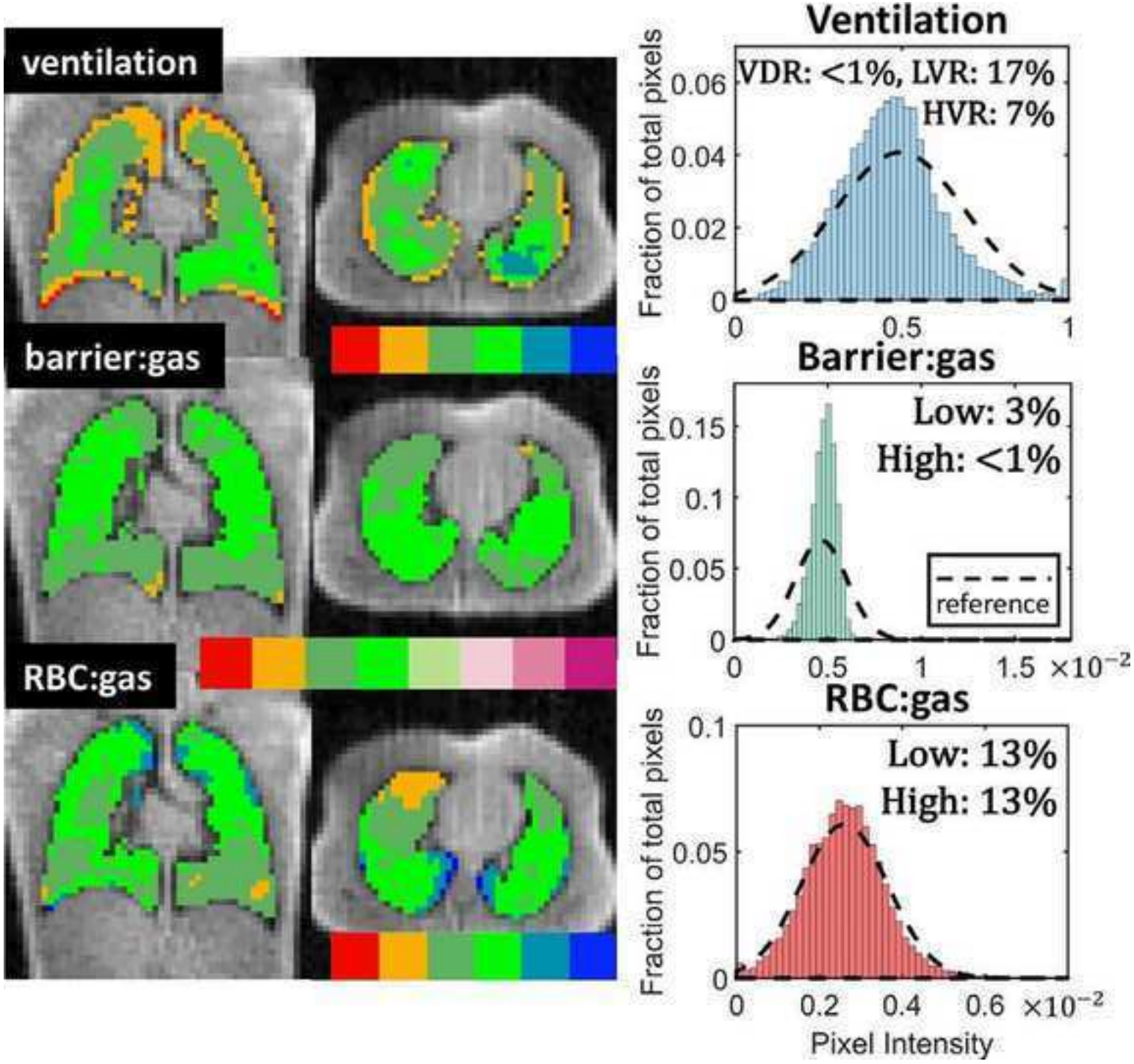

Figure 11 (right)

Click here to access/download;Figure;Figure new11_RIGHT.jpg

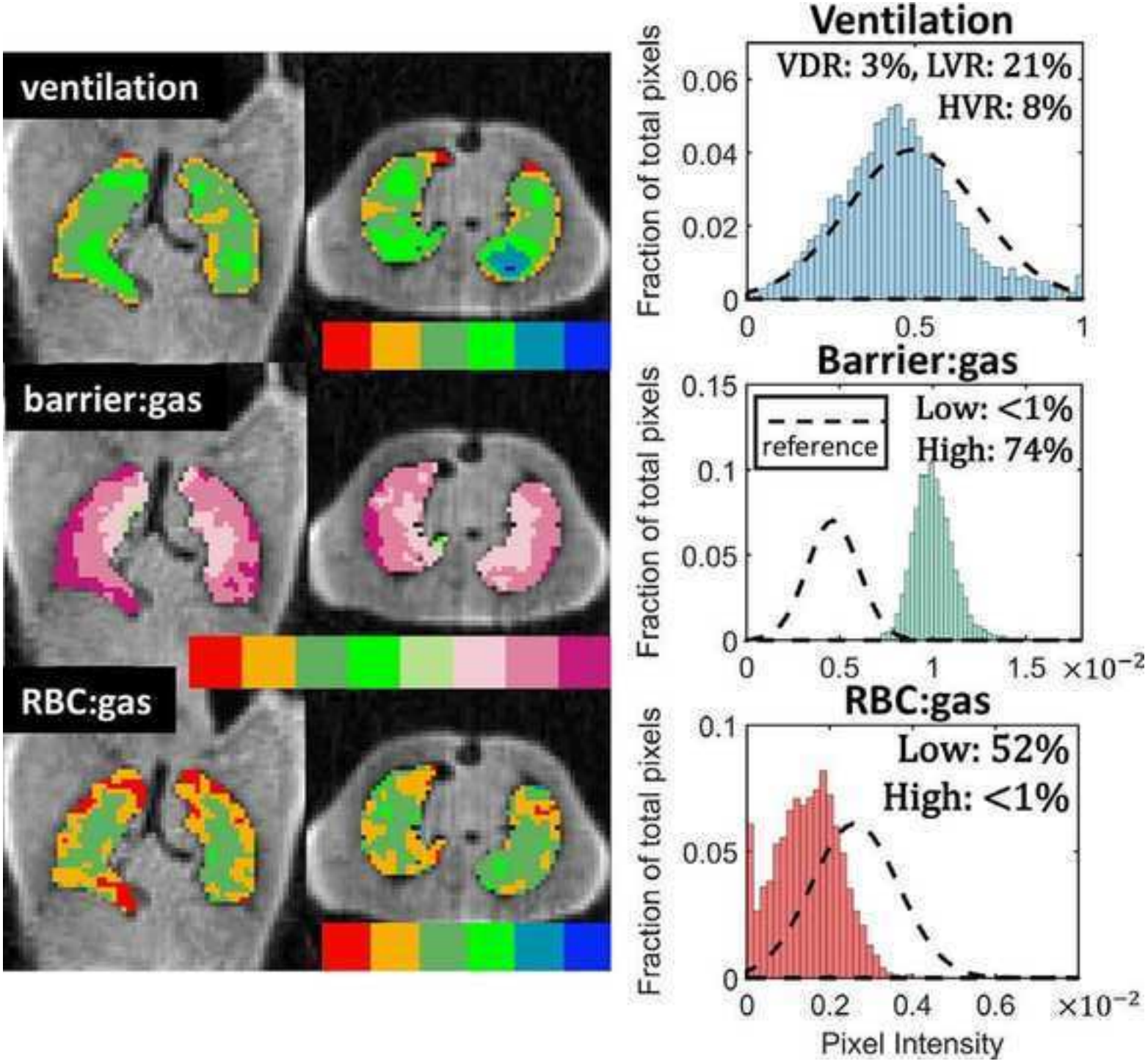

Figure 12

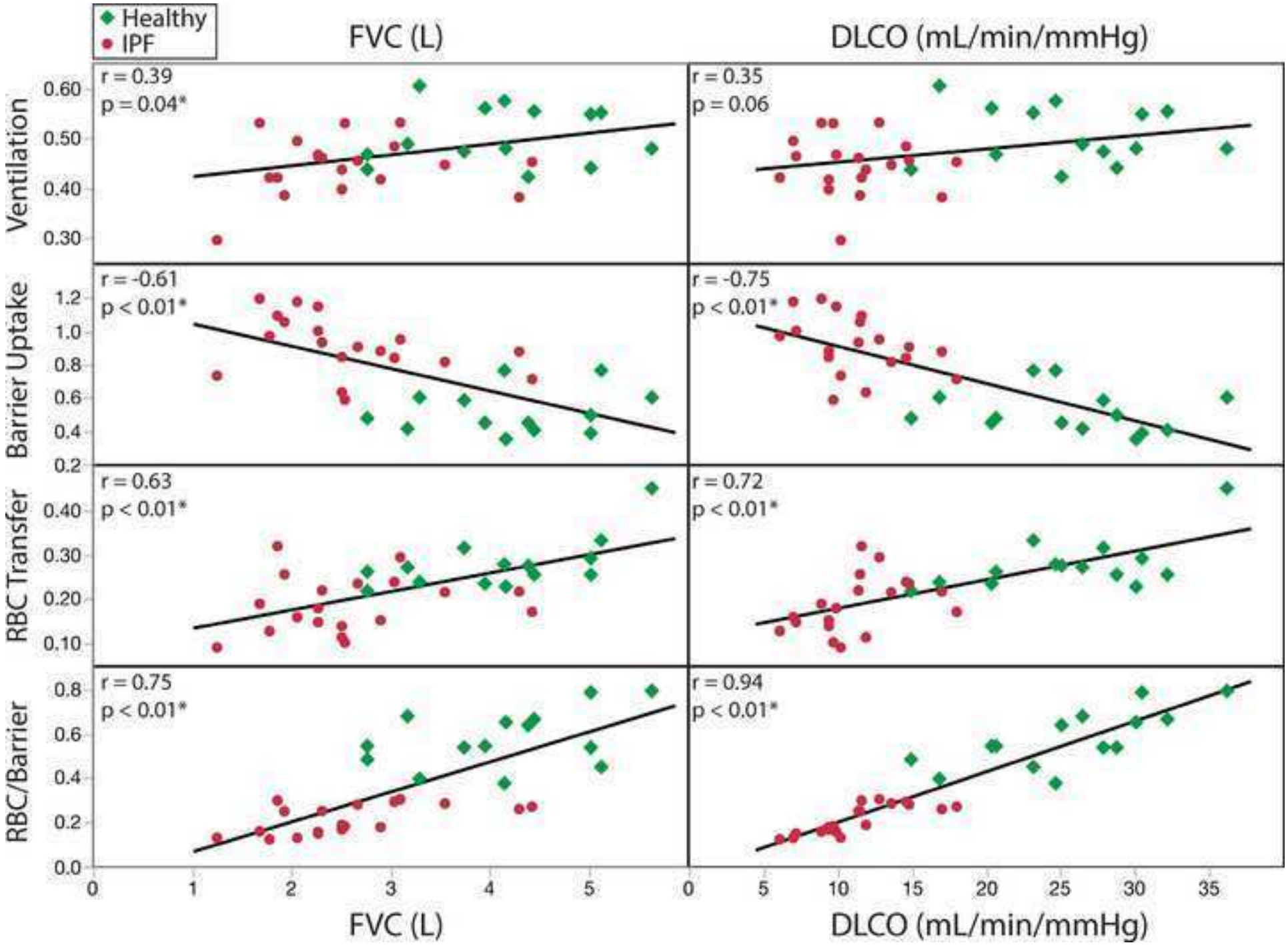

Figure 13

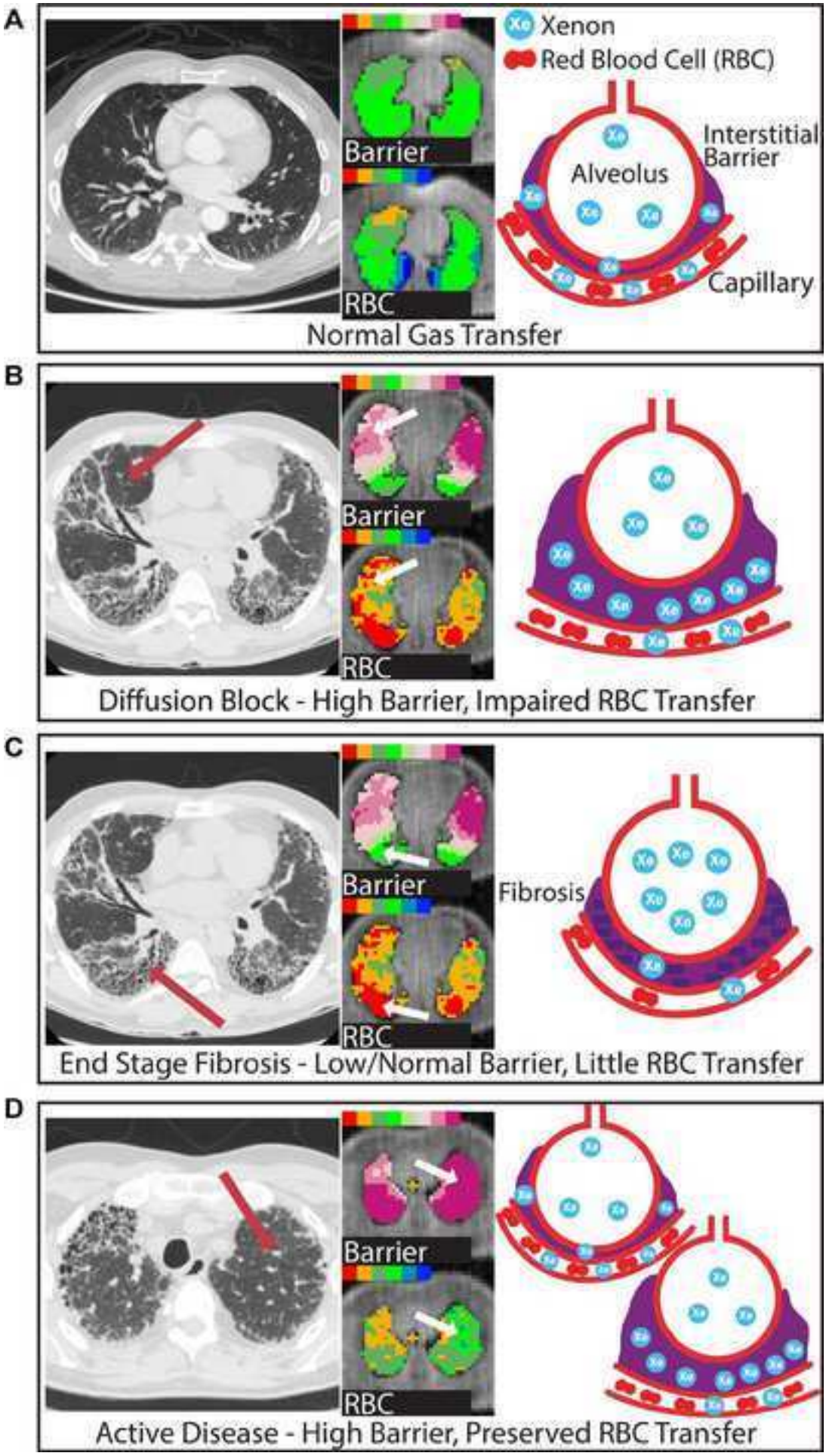

Figure 14

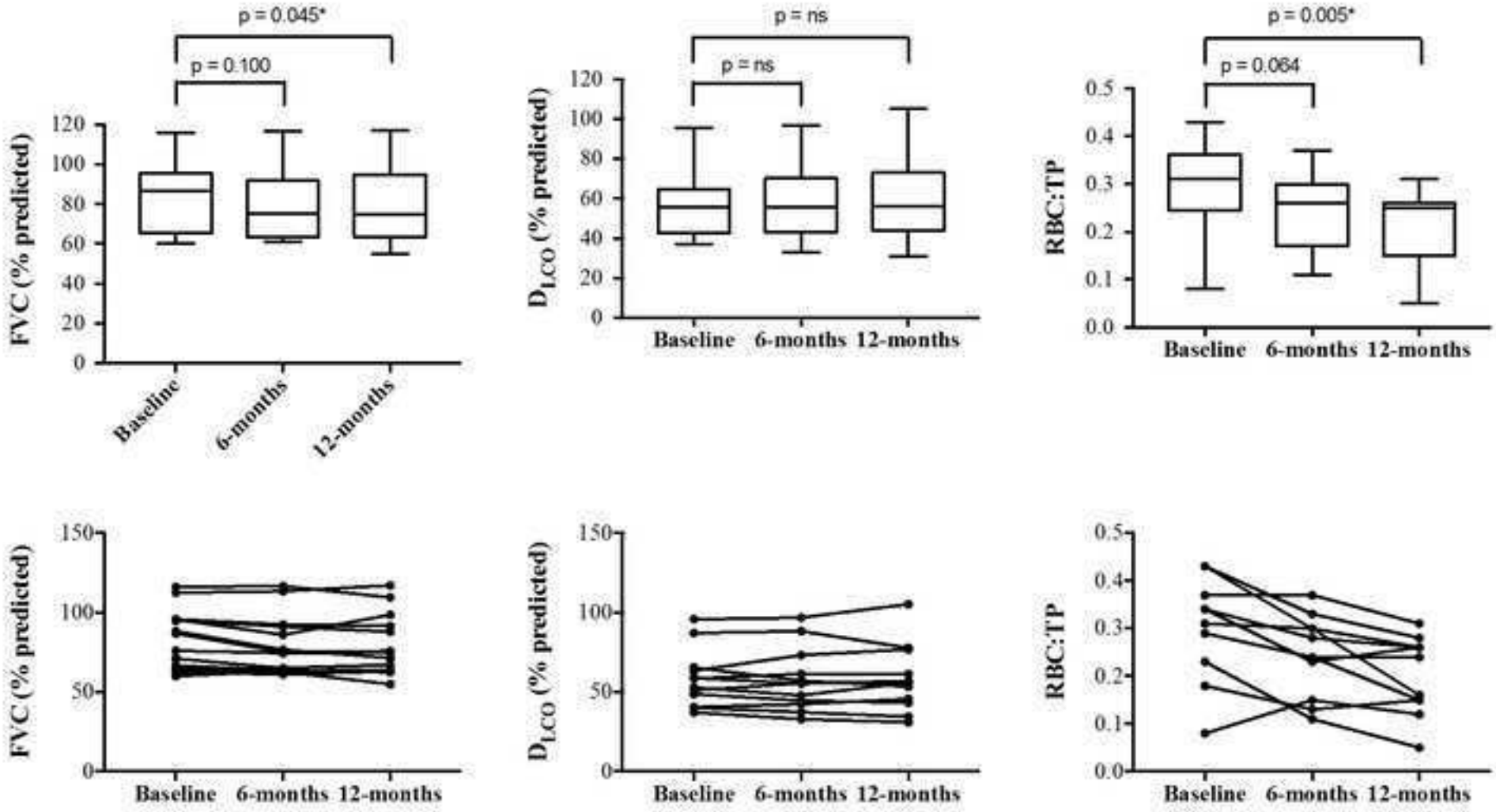

Figure 15